NOAA Atlas NESDIS 90

WORLD OCEAN ATLAS 2023
Volume 2: Salinity

Silver Spring, MD
February 2024

U.S. DEPARTMENT OF COMMERCE
National Oceanic and Atmospheric Administration
National Environmental Satellite, Data, and Information Service
National Centers for Environmental Information

For updates on the data, documentation, and additional information about the WOA23 please refer to:
https://www.ncei.noaa.gov/products/world-ocean-atlas

This document is available on line at https://www.ncei.noaa.gov/products/world-ocean-atlas

WORLD OCEAN ATLAS 2023
Volume 2: Salinity

James R. Reagan, Dan Seidov, Zhankun Wang, Dmitry Dukhovskoy,
Timothy P. Boyer, Ricardo A. Locarnini, Olga K. Baranova,
Alexey V. Mishonov, Hernan E. Garcia, Courtney Bouchard, Scott L. Cross,
and Christopher R. Paver

Technical Editor: Alexey Mishonov

Ocean Climate Laboratory
National Centers for Environmental Information

Silver Spring, Maryland
February 2024

U.S. DEPARTMENT OF COMMERCE
Gina M. Raimondo, Secretary

National Oceanic and Atmospheric Administration
Richard W. Spinrad, Under Secretary of Commerce for Oceans and
Atmosphere and NOAA Administrator

National Environmental Satellite, Data and Information Service
Stephen Volz, Assistant Administrator

To Sydney (Syd) Levitus

Syd exemplifies the craft of careful, systematic inquiry of the large-scale distributions and low-frequency variability from seasonal-to-decadal time scales of ocean properties. He was one of the first to recognize the importance and benefits of creating objectively analyzed climatological fields of measured ocean variables including temperature, salinity, oxygen, nutrients, and derived fields such as mixed layer depth. Upon publishing *Climatological Atlas of the World Ocean* in 1982, he distributed this work without restriction, an act not common at the time. This seminal atlas moved the oceanographic diagnostic research from using hand-drawn maps to using objectively analyzed fields of ocean variables.

With his NODC (now NCEI) Ocean Climate Laboratory (OCL) colleagues, and unprecedented cooperation from the U.S. and international ocean scientific and data management communities, he created the *World Ocean Database (WOD)*; the world's largest collection of ocean profile data that are available internationally without restriction. The *World Ocean Atlas (WOA)* series represents the gridded objective analyses of the WOD and these fields have also been made available without restriction.

The WOD and WOA series are used so frequently that they have become known generically as the "Levitus Climatology". These databases and products enable systematic studies of ocean variability in its climatological context that were not previously possible. His foresight in creating WOD and WOA has been demonstrated by their widespread use over the years. Syd has made major contributions to the scientific and ocean data management communities. He has also increased public understanding of the role of the oceans in climate. He retired in 2013 after 39 years of distinguished civil service. He distilled the notion of the synergy between rigorous data management and science; there are no shortcuts.

All of us at the Ocean Climate Laboratory would like to once again dedicate this atlas to Syd, his legacy, vision, and mentorship.

The OCL Team

Table of Contents

List of Figures

List of Tables

List of Acronyms

Acronym	Expanded Term
APB	Autonomous Pinniped Bathythermograph
BAMS	Bulletin of the American Meteorological Society
CSV	Comma-Separated Value
CTD	Conductivity Temperature Depth
DBT	Drifting Bathythermograph
DOC	Department of Commerce
DOE	Department of Energy
DRB	Drifting Buoy
ENSO	El Niño-Southern Oscillation
ERL	Earth Research Laboratory
ETOPO2	Earth Topography 2 arc minute
EVR	Extended Vertical Resolution
GIS	Geographic Information System
GLD	Glider
GMT	Greenwich Mean Time, or Generic Mapping Tools
GODAR	Global Ocean Data Archaeology and Rescue
GTSPP	Global Temperature-Salinity Profile Program
IAPSO	International Association for the Physical Sciences of the Oceans
IOC	International Oceanographic Commission
IODE	International Oceanographic Data Exchange
IRI	International Research Institute for Climate and Society
JAMSTEC	Japan Agency for Marine-Earth Science and Technology
JPOTS	Joint Panel on Oceanographic Tables and Standards
LDEO	Lamont-Doherty Earth Observatory
MAST	Marine Science and Technology
MBT	Mechanical Bathythermograph
MEDAR	Mediterranean Data Archeology and Rescue
MRB	Moored Buoy
NAO	North Atlantic Oscillation
NASA	National Aeronautics and Space Administration
NATO	North Atlantic Treaty Organization
NCEI	National Centers for Environmental Information
NESDIS	National Environmental Satellite, Data, and Information Service
NOAA	National Oceanic and Atmospheric Administration

Acronym	Expanded Term
NODC	National Ocean Data Center
OCL	Ocean Climate Laboratory
ODV	Ocean Data View
PFL	Profiling Float
PIRATA	Prediction and Research Moored Array in the Tropical Atlantic
PSS	Practical Salinity Scale
RAMA	Research Moored Array for African-Asian-Australian Monsoon Analysis and Prediction
RDML	Rear Admiral
SST	Sea Surface Temperature
SUR	Surface
TAO/TRITON	Tropical Atmosphere Ocean moored buoy array
TSK	Tsurumi-Seiki Company
UNESCO	United Nations Educational, Scientific and Cultural Organization
UOR	Undulating Oceanographic Recorder
USA	United States of America
USN	United States Navy
WDS	World Data Service
WOA	World Ocean Atlas
WOD	World Ocean Database
XBT	eXpendable BathyThermograph
XCTD	eXpendable Conductivity Temperature Depth

Preface

The World Ocean Atlas 2023 (WOA23) is the latest in a line of oceanographic analyses of subsurface ocean variables at standard depths extending back to the groundbreaking *Climatological Atlas of the World Ocean* (Levitus, 1982). The WOA has been published semi-regularly since 1994, with versions in 1998, 2001, 2005, 2009, 2013, 2018 and now 2023. Previous iterations of the WOA have proven to be of great utility to the oceanographic, climate research, geophysical, and operational environmental forecasting communities. The oceanographic variable analyses are used as boundary and/or initial conditions in numerical ocean circulation models and atmosphere-ocean models, for verification of numerical simulations of the ocean, as a form of "sea truth" for satellite measurements such as altimetric observations of sea surface height, for computation of nutrient fluxes by Ekman transport, and for planning oceanographic expeditions among others.

WOA23 includes analyses on a one-degree grid for all variables and on a quarter-degree grid for temperature and salinity. Since WOA13, the ocean variable analyses are produced on 102 depth levels from the surface to 5,500 m (previously 33 levels within the same depth limits). Ocean data and analyses of data at higher vertical resolution than previously available are needed to document the variability of the ocean, including improving diagnostics, understanding, and modeling of the physics of the ocean.

In the acknowledgment section of this publication, we have expressed our view that creation of global ocean profile and plankton databases and analyses are only possible through the cooperation of scientists, data managers, and scientific administrators throughout the international scientific community.

WOA23 was made available in February, 2024.

Ocean Climate Laboratory Team
National Centers for Environmental Information
Silver Spring, MD
February 2024

Acknowledgments

We dedicate this work to Carla Coleman who always contributed with a smile and was taken from us too soon.

WORLD OCEAN ATLAS 2023
Volume 2: Salinity

ABSTRACT

This atlas consists of a description of data analysis procedures and horizontal maps of climatological distribution fields of salinity at selected standard depth levels of the World Ocean on a one-degree and quarter-degree latitude-longitude grids. The aim of the maps is to illustrate large-scale characteristics of the variability in ocean salinity. The fields used to generate these climatological maps were computed by objective analysis of all scientifically quality-controlled historical salinity data in the *World Ocean Database 2023*. Maps are presented for climatological composite periods: annual and seasonal at 102 standard depths, and monthly at 57 standard depths.

1. INTRODUCTION

This atlas is part of the *World Ocean Atlas 2023* (WOA23) series. The WOA23 series includes analysis for temperature (Locarnini *et al.*, 2024); salinity (this atlas); dissolved oxygen (Garcia *et al.*, 2024a); dissolved inorganic nutrients (Garcia *et al.*, 2024b); conductivity (Reagan *et al.*, 2024a); density (Locarnini *et al.*, 2024b); mixed layer depth (Wang *et al.,* 2024); and bottom temperature (Mishonov *et al.,* 2024b). This atlas presents annual, seasonal, and monthly climatologies and related statistical fields for salinity. Climatologies in this atlas are defined as mean oceanographic fields at selected standard depth levels based on the objective analysis of historical oceanographic profiles and select surface-only data. A profile is defined as a set of measurements for a single variable (temperature, salinity, *etc.*) at discrete depths taken as an instrument drops or rises vertically in the water column. Temperature and salinity climatologies are comprised of seven "decadal" climatologies for the following time periods: 1955-1964, 1965-1974, 1975-1984, 1985-1994, 1995-2004, 2005-2014, and 2015-2022 as well as three successive 30-year "climate normal" periods: 1971-2000, 1981-2010, and 1991-2020. A "climate normal" is a 30-year

average of a particular variable of the climate system and is defined by the World Meteorological Organization (WMO, 2017). The current climate normal (*i.e.,* 1991-2020) helps establish a baseline to compare present day observations to. It also describes the current state of the climate and what one might expect to see during different times of the year. The annual "all-data" climatology was calculated using observations from all months of all years. Seasonal "all-data" climatologies were calculated using only data from the defined season (regardless of year). The seasons are defined as follows: Winter is defined as January, February, and March; spring as April, May, and June; summer as July, August, and September; and fall as October, November, and December. Monthly "all-data" climatologies were calculated using data only from the given month. Finally, a seven-decade average climatology for temperature and salinity (named 'decav') is also provided that is calculated by averaging all seven individual decades (1955-1964 through 2015-2022) together.

The salinity data used are available from the National Centers for Environmental Information (NCEI; formerly National Oceanographic Data Center) and World Data Service (WDS) for Oceanography, Silver Spring, Maryland. Large volumes of data

have been acquired as a result of the fulfillment of several data management projects including:

a) the Intergovernmental Oceanographic Commission (IOC) Global Oceanographic Data Archaeology and Rescue (GODAR) project (Levitus 2012);
b) the IOC World Ocean Database project (WOD);
c) the IOC Global Temperature Salinity Profile project (GTSPP) (IOC, 1998).
d) the Argo program, part of the Global Ocean Observing System (Argo, 2000)

The salinity data used in the WOA23 have been analyzed in a consistent, objective manner on one-degree and quarter-degree latitude-longitude grids at standard depth levels from the surface to a maximum depth of 5500m. The procedures for "all-data" climatologies are identical to those used in the *World Ocean Atlas 2018* (WOA18) series (Locarnini *et al*. 2019; Zweng *et al*., 2019; Garcia *et al.,* 2019a,b), *World Ocean Atlas 2013* (WOA13) series (Locarnini *et al*. 2013; Zweng *et al*., 2013; Garcia *et al.,* 2013a,b), *World Ocean Atlas 2009* (WOA09) series (Locarnini *et al*., 2010; Antonov *et al*., 2010; Garcia *et al*. 2010a,b), *World Ocean Atlas 2005* (WOA05) series (Locarnini *et al*., 2006; Antonov *et al*., 2006; Garcia *et al*. 2006a,b), the *World Ocean Atlas 2001* (WOA01) series (Stephens *et al.*, 2002; Boyer *et al*., 2002; Locarnini *et al.*, 2002; Conkright *et al*., 2002) and *World Ocean Atlas 1998* (WOA98) series (Antonov *et al*., 1998a,b,c; Boyer *et al*., 1998a,b,c; Conkright *et al*., 1998a,b,c; O'Brien *et al*., 1998a,b,c). Slightly different procedures were followed in earlier analyses (Levitus, 1982; *World Ocean Atlas 1994* series [WOA94, Levitus and Boyer 1994a,b; Levitus *et al*., 1994c; Conkright *et al*., 1994]). WOA13 differed from WOA09 by increasing the number of standard levels used from 33 to 102, increasing the resolution with

depth; WOA23 continues to use the same 102 depth levels as WOA13 and WOA18.

Objective analyses shown in this atlas are limited by the nature of the salinity database (data are non-uniform in both space and time), characteristics of the objective analysis techniques, and the grid used. The primary limitation of the analysis is data coverage in space and time. Since the publication of WOA18, substantial amounts of additional historical salinity data have become available. However, even with these additional data, we are still hampered in a number of ways by a lack of data. In some areas, quality control is made difficult by the limited amount of data collected in these areas. Data may exist in an area for only one season, thus precluding any representative annual analysis. In some areas there may be a reasonable spatial distribution of data points on which to base an analysis, but there may be only a few (perhaps only one) data values in each one-degree latitude-longitude square.

This atlas is divided into sections. We begin by describing the data sources and data distribution (Section 2). Then we describe the general data processing procedures (Section 3), the results (Section 4), summary (Section 5), and future work (Section 6). After the references (Section 7), the appendices of this atlas (Section 8) include descriptions and examples of the stabilization of the temperature and salinity climatologies. Maps for each individual depth level for each time period are available online.

2. DATA SOURCES AND DATA DISTRIBUTION

Data sources and quality control procedures are briefly described below. For further information on the data sources used in WOA23 refer to the *World Ocean Database 2023* (WOD23, Mishonov *et al.*, 2024a). The quality control procedures used in

preparation of these analyses are described in Garcia *et al.* (2024c).

2.1. Data sources

Historical oceanographic salinity profile data from bottle samples, ship-deployed Conductivity-Temperature-Depth (CTD) packages, profiling floats, moored and drifting buoys, gliders, and undulating oceanographic recorder (UOR) profiles used in this project were obtained from the NCEI/WDS archives and include all data gathered as a result of the GODAR and WOD projects.

An important source of near-surface salinity data is ship-mounted thermosalinographs, which measure surface temperature and salinity as ships transit the ocean. While the primary focus of WOD and WOA is profile and subsurface data, we have included some thermosalinograph data in the climatological salinity analysis as part of the SUR (surface) dataset. For further information, please see Chapter 14 of the WOD23 documentation (Mishonov *et al.*, 2024a).

To understand the procedures for taking individual oceanographic observations and constructing climatological fields, it is necessary to define the terms "standard level data" and "observed level data". We refer to the actual measured in situ value of an oceanographic variable as an "observation", and to the depth at which such a measurement was made as the "observed level depth." We refer to such data as "observed level data." Before the development of oceanographic instrumentation that measures at high frequencies along the vertical profile, oceanographers often attempted to make measurements at selected "standard levels" in the water column. Sverdrup *et al.* (1942) presented the suggestions to the International Association for the Physical Sciences of the Oceans (IAPSO) as to which depths

oceanographic measurements should be made or interpolated to for analysis. Historically, the World Ocean Atlas used a modified version of the IAPSO standard depths. However, with the increased global coverage of high depth resolution instrumentation, such as profiling floats, WOA has extended the number of standard depth levels from 33 to 102. The current standard depth levels include the original depth levels presented up to WOA09, but have tripled the resolution in the upper 100 meters, more than doubled the depth resolution of the upper 1000 meters, and more than tripled the depth resolution between 1000 and 5500 meters. For many purposes, including preparation of the present climatologies, observed level data are interpolated to standard depth levels if observations did not occur at the desired standard depths (see section 3.1 for details). The levels at which the climatologies were calculated are given in Table 2. Table 3 describes the datasets used to calculate the climatologies. Table 4 shows the depths of each standard depth level.

The *World Ocean Database 2023* (WOD23) is set to be released by the end of March 2024. WOD23 will contain all in situ ocean profiles assembled and processed by the Ocean Climate Laboratory team at the National Centers for Environmental Information through December 2022. This includes all Argo measurements made by December 31, 2022, with quality control as of April 1, 2023. Additionally, WOD23 will contain updated quality control flags based on the quality improvements made during the construction of the *World Ocean Atlas 2023*. These are further discussed in section 2.2 of this document. Finally, WOA23 will be completely reproducible from the data within the WOD23.

2.2. Data quality control

Quality control of the salinity data is a major task, the difficulty of which is directly related to lack of data and metadata (for some areas) upon which to base statistical checks. Consequently, certain empirical criteria were applied - see sections 2.2.1 through 2.2.4, and as part of the last processing step, subjective judgment was used - see sections 2.2.5 and 2.2.6. Individual salinity data, and in some cases entire profiles or all profiles for individual cruises, have been flagged and not used further because these data produced features that were judged to be non-representative or questionable. As part of our work, we will make available WOD23 that contains both observed levels profile data and standard depth level profile data with various quality control flags applied. The flags mark either individual measurements or entire profiles that were not used in the next step of the procedure -- either interpolation to standard depth levels for observed level data or calculation of statistical means in the case of standard depth level data.

Constantly improving knowledge of the world ocean variability now includes a greater appreciation and understanding of the ubiquity of mesoscale features such as eddies, rings, and lenses in some parts of the world ocean, as well as interannual and multi-decadal variability of water mass properties associated with modal variability of the climate system such as the North Atlantic Oscillation (NAO) and El Niño Southern Ocean Oscillation (ENSO). Some of these features, especially in regions with dense data coverage like the Northwest Atlantic Ocean, can find their way into high-resolution analyses and lead to a cumulative effect of mesoscale dynamics seen in decadal climatologies (Seidov *et al.,* 2018). However, in most regions with lesser data coverage, these features are seen as outliers and may not be consistent with the background WOA fields, but still represent legitimate data

values. Therefore, we have simply flagged these data, if seen as obvious outliers, but have not removed them from the WOD23. Thus, individual investigators can make their own decision regarding the representativeness of the data. Investigators studying the distribution of features such as eddies will be interested in those data that we may regard as unrepresentative for the preparation of the analyses shown in this atlas.

2.2.1. Duplicate elimination

Because salinity data are received from many sources, sometimes the same data set is received at NCEI/WDS more than once but with slightly different time and/or position and/or data values, and hence are not easily identified as duplicate stations. Therefore, to eliminate the repetitive data values, our databases were checked for the presence of exact and "near" exact replicates using eight different criteria. The first checks involve identifying stations with exact position/date/time and data values; the next checks involve offsets in position/date/time. Profiles identified as duplicates in the checks with a large offset were individually verified to ensure they were indeed duplicate profiles.

All but one profile from each set of duplicate profiles were removed at the first step of our processing.

2.2.2. Range and gradient checks

Range checking (that is, checking whether a salinity value is within preset minimum and maximum values as a function of depth and major ocean basin) was performed on all salinity values as a first quality control check to flag and withhold from further use the relatively few values that were grossly outside expected oceanic ranges. Range checks were prepared for individual regions of the world ocean. Garcia *et al.* (2024c) and Boyer and Levitus (1994) detail the quality

control procedures. Range tables showing the salinity ranges selected for each basin and depth can be found in Garcia *et al*. (2024c).

A check as to whether excessive vertical gradients occur in the data has been performed for each variable in WOD23 both in terms of positive and negative gradients. See Garcia *et al.* (2024c) for limits for excessive gradients for salinity.

2.2.3. Statistical checks

Statistical checks were performed on the data according to the following procedure. All data for salinity (irrespective of year), at each standard depth level, were averaged within five-degree latitude-longitude squares to produce a record of the number of observations, mean, and standard deviation in each square. Statistics were computed for the annual, seasonal, and monthly compositing periods. For each iteration of the World Ocean Atlas, all statistical flags applied in previous WOA products (*e.g.,* WOA18) were cleared and new statistical flags were produced. Below 50 m depth, if data were more than three standard deviations from the mean, the data were flagged and withheld from further use in the objective analyses. The three standard deviation check is for the subsurface open ocean where we expect the least variability; we use relatively looser checks in areas where variability is higher. Above 50 m depth, a five-standard-deviation criterion was used in five-degree squares that contained any land area. In selected one-degree squares that are close to land areas, a four-standard-deviation check was used. In all other squares, a three-standard-deviation criterion was used for the 0-50 m depth layer. For standard depth levels situated directly above the bottom, a four-standard-deviation criterion was used.

The reason for the weaker standard deviation criterion in coastal and near-coastal regions is the large variability in the coastal five-degree square statistics for some variables. Frequency distributions of some variables in some coastal regions are skewed or bimodal. Thus, to avoid eliminating possibly good data in highly variable environments, the standard deviation criteria were broadened.

The total number of measurements in each profile and the total number of salinity observations exceeding the criterion is recorded. If more than four standard level values in a profile were found to exceed the standard deviation criterion, then the entire profile was flagged. This check was imposed after tests indicated that surface data from particular casts (which upon inspection appeared to be erroneous) were being flagged but deeper data were not. Other situations were found where erroneous data from the deeper portion of a cast were flagged, while near-surface data from the same cast were not flagged because of larger natural variability in surface layers. One reason for this was the decrease in the number of observations with depth and the resulting change in sample statistics. The standard-deviation check was applied twice to the data set for each compositing period.

In summary, first the five-degree square statistics were computed, and the data flagging procedure described above was used to provide a preliminary data set. Next, new five-degree-square statistics were computed from this preliminary data set and used with the same statistical check to produce a new, "clean" data set. The reason for applying the statistical check twice was to flag (and withhold from further use), in the first round, any grossly erroneous or non-representative data from the data set that would artificially increase the variances. The second check is then more effective in identifying values with smaller differences that are still non-representative.

2.2.4. Static stability check

In addition to standard level statistical checks, each cast containing both temperature and salinity was checked for static stability as defined by Hesselberg and Sverdrup (1914). Neumann and Pierson (1966, p. 139) reviewed this definition. The computation is a "local" one in the sense that adiabatic displacements between adjacent temperature-salinity measurements in the vertical are considered rather than displacements to the sea surface. Lynn and Reid (1968) discussed the reasons for use of the local stability computation. The procedure for computation follows that used by Lynn and Reid (1968) and is given by:

$$E = \lim_{\partial z \to 0} \frac{1}{\rho_0} \frac{\delta \rho}{\partial z}$$

in which: $\rho_o = 1.02$ g·cm^{-3}. As noted by Lynn and Reid (1968), the term (E) "is the individual density gradient defined by vertical displacement of a water parcel (as opposed to the geometric density gradient). For discrete samples the density difference ($\delta \rho$) between two samples is taken after one is adiabatically displaced to the depth of the other". For the results at any standard level (k), the computation was performed by displacing parcels at the next deeper standard level ($k+1$) to level k.

The actual procedure for using stability checks to flag sets of data points was as follows. To a depth of 30 m, stability (E) inversions in excess of $3 \cdot 10^{-5}$g·cm^{-3} were flagged, and below this depth down to the 400m level, inversions in excess of $2 \cdot 10^{-5}$g·cm^{-3} were flagged. Below 400m any inversion was flagged. To eliminate an inversion, both temperature and salinity were flagged and eliminated from further use at both standard levels involved in the computation. In the actual processing, a count was kept for the number of inversions in each cast. If a cast had two or more unacceptable inversions, as defined above, then the entire cast was flagged and eliminated from further use.

2.2.5. Subjective flagging of data

Analysis for WOA23 was done on two grids: a one-degree grid and a quarter-degree grid. For the one-degree analysis, the salinity data were averaged by one-degree squares for input to the objective analysis program. After initial objective analyses were computed, the input set of one-degree means still contained questionable data contributing to unrealistic distributions, yielding intense bullseyes or spatial gradients. Examination of these features indicated that some of them were due to profiles from particular oceanographic cruises. In such cases, data from an entire cruise were flagged and withheld from further use by setting a flag on each profile from the cruise. In other cases, individual profiles or measurements were found to cause these features and were flagged. For the quarter-degree analysis, the same procedure was repeated on a finer quarter-degree grid.

2.2.6. Representativeness of the data

Another quality control issue is data representativeness. The general paucity of data forces the compositing of all historical data to produce "climatological" fields. In a given grid square, there may be data from a month or season of one particular year, while in the same or a nearby square there may be data from an entirely different year. If there is large interannual variability in a region where scattered sampling in time has occurred then one can expect the analysis to reflect this. Because the observations are scattered randomly with respect to time, except for a few limited areas, the results cannot, in a strict sense, be considered a true long-term climatological average.

The WOA23 is comprised of smoothed fields from analyses of historical means, based (in

certain areas) on relatively few observations. We believe, however, that useful information about the oceans can be gained through our procedures and that the large-scale and even mesoscale features (in ¼-degree analyses) are representative of the real ocean.

The data diminish in number with increasing depth. In the upper ocean, the all-data annual mean distributions are sufficient for defining large-scale features, but the database is inadequate in some regions for the seasonal periods. In some areas of the deep ocean, the distribution of observations may be adequate for some diagnostic computations but inadequate for other purposes. If an isolated deep basin or some region of the deep ocean has only one observation, then no horizontal gradient computations are meaningful. However, useful information is provided by the observation in the computation of other quantities (*e.g.* a volumetric mean over a major ocean basin).

2.2.7. XCTD drop-rate error correction

Johnson (1995) has shown the necessity of depth correction for Sippican XCTDs, while Mizuno and Watanabe (1998) and Koso *et al*. (2005) give depth corrections for TSK XCTDs. Kizu *et al*. (2008) found that the TSK manufacturer's drop rate as corrected according to these works is generally satisfactory. **We have made no correction to the depths of the observed level XCTD profiles**. Thus, investigators, if they desire, can make whatever correction they need to the observed level data we are providing since we have not corrected these profiles for this error. However, in order to merge Sippican and TSK XCTD data with other types of salinity measurements, and in order to produce climatologies and other analyses, by necessity we have corrected the drop-rate error in these XCTD profiles, as part of the process of interpolating the data to standard depth levels (the drop-rate correction was applied to the observed level data before

interpolation to standard levels). **All Sippican and TSK XCTD profiles that we have used in generating products at standard levels, or made available as part of our standard level profile data sets, have been corrected for the drop-rate error**. **If users wish to use another procedure, but still use the XCTD data set we have compiled, they can do so by applying their correction procedure to our observed level XCTD profile data set, which has not been corrected for the drop-rate error**.

2.2.8. Exclusion of real-time Argo profiling float salinity data

WOD23 contains ~2.6 million Argo profiling float salinity casts. Most of these casts were taken post-2000, with near-global Argo coverage occurring in ~2005 and continuing through 2022. It has been the dominate ocean observing system since the early 2000's.

Argo profiling floats can observe bias salinity measurements, of which the conductivity cell sensor drift (Wong *et al.,* 2020) is the most substantial source of Argo salinity error. The Argo community can identify profiling floats suffering from this drift, and in many cases correct them with an adjustment. Historically, about ~10% of the Argo salinity data have been identified as having an adjustable salty bias (Wong *et al*., 2023). A prominent salty bias (~0.004) was identified by the Argo community during the 2015-2020 period that was attributed to a CTD manufacturer defect. This salty bias peaked in 2017-2018 where there were roughly ~17% of Argo profiling floats identified as having an adjustable salty bias (Wong *et al*., 2023).

Argo salinity data go through rigorous quality control checks as discussed in Wong et al. (2022; 2023). Argo salinity data within WOD23 can be divided into real-time, real-time adjusted, and delayed-mode. The delayed-mode data are the highest quality

and are only available 12-18 months after the time the raw (i.e., real-time) measurements were observed (Wong *et al.*, 2023). If the delayed-mode salinity data were adjusted (even if the adjustment was 0.0), this will be documented. The real-time adjusted Argo salinity data are available immediately and are adjusted based on carrying forward the (if available) delayed-mode adjustment for that float. If there is no delayed-mode adjustment documented for that float, then the data will be considered real-time with no adjustment. We have found that the real-time adjustments and delayed-mode adjustments have tracked very similar to one another since 2005.

Thus, since a bias in Argo salinity can exist in some of the real-time data that have not been adjusted, we have decided to eliminate all real-time Argo salinity data from the climatological calculations. This resulted in the loss of about 5.6%, or ~145,000 of 2.6 million, Argo salinity profiles from our analyses. However, the real-time Argo salinity data is still available in WOD23 if users would like to use this data in their analysis.

3. DATA PROCESSING PROCEDURES

3.1. Vertical interpolation to standard levels

Vertical interpolation of observed depth level data to standard depth levels followed procedures in JPOTS Editorial Panel (1991). These procedures are in part based on the work of Reiniger and Ross (1968). Four observed depth level values surrounding the standard depth level value were used, two values from above the standard level and two values from below the standard level. The pair of values furthest from the standard level is termed "exterior" points and the pair of values closest to the standard level is termed "interior" points. Paired parabolas were

generated via Lagrangian interpolation. A reference curve was fitted to the four data points and used to define unacceptable interpolations caused by "overshooting" in the interpolation. When there were too few data points above or below the standard level to apply the Reiniger and Ross technique, we used a three-point Lagrangian interpolation. If three points were not available (either two above and one below or vice-versa), we used linear interpolation. In the event that an observation occurred exactly at the depth of a standard level, then a direct substitution was made. Table 4 provides the range of acceptable distances for which observed level data could be used for interpolation to a standard level.

WOD13 increased the number of standard levels from 33 to 102, allowing for analysis with greater vertical resolution. WOA23 also uses 102 standard depth levels. The method for interpolating data to standard levels remains the same as previous analyses.

3.2. Methods of analysis

3.2.1. Overview

An objective analysis scheme similar to the one in Barnes (1964) was used to produce the fields shown in this atlas. This scheme had its origins in the work of Cressman (1959). In *World Ocean Atlas 1994* (WOA94), the Barnes (1973) scheme was used. This required only one "correction" to the first-guess field at each grid point in comparison to the successive correction method of Cressman (1959) and Barnes (1964). This was to minimize computing time used in the processing. Barnes (1994) recommended a return to a multi-pass analysis when computing time is not an issue. Based on our own experience we agree with this assessment. The single pass analysis, used in WOA94, caused an artificial front in the Southeastern Pacific Ocean in a data sparse area (Anne Marie Treguier, personal

8

communication). The analysis scheme used in generating WOA98, WOA01, WOA05, WOA09, WOA13, WOA18, and WOA23 analyses uses a three-pass "correction" which does not result in the creation of this artificial front.

The analysis was performed on both the one-degree and quarter-degree grids. Inputs to the analysis scheme were one grid square means of data values at standard levels (for time period and variable being analyzed), and a first-guess value for each square. For instance, grid-square means for our "all-data" annual analysis were computed using all available data regardless of date of observation. For "all-data" July, we used all historical July data regardless of year of observation. For "decadal" July, we used July data only collected within a specified decade.

Analysis was the same for all standard depth levels. Each one- or quarter-degree latitude-longitude square value was defined as being representative of its square. The dimension of the one-degree grid was 360x180, while the quarter-degree grid was 1440x720. Grid points are located at the "centers" of their boxes. An influence radius (choice of the radius is discussed in section 3.2.4) was then specified. At those grid points where there was an observed mean value, the difference between the mean and the first-guess field was computed. Next, a correction to the first-guess value at all grid points was computed as a distance-weighted mean of all grid point difference values that lie within the area around the grid point defined by the influence radius. Mathematically, the correction factor derived by Barnes (1964) is given by the expression:

$$C_{i,j} = \frac{\sum_{s=1}^{n} W_s Q_s}{\sum_{s=1}^{n} W_s} \qquad (1)$$

in which:

(i,j) - coordinates of a grid point in the east-west and north-south directions respectively;

$C_{i,j}$ - the correction factor at grid point coordinates (i,j);

n - the number of observations that fall within the area around the point i,j defined by the influence radius;

Q_s - the difference between the observed mean and the first-guess at the Sth point in the influence area;

$$W_s = e^{-\frac{Er^2}{R^2}} \text{ (for } r \leq R; W_s = 0 \text{ for } r > R);$$

r - distance of the observation from the grid point;

R - influence radius;

$E = 4$.

The derivation of the weight function, W_s, will be presented in the following section. At each grid point we computed an analyzed value $G_{i,j}$ as the sum of the first-guess, $F_{i,j}$, and the correction $C_{i,j}$. The expression for this is

$$G_{i,j} = F_{i,j} + C_{i,j} \qquad (2)$$

If there were no data points within the area defined by the influence radius, then the correction was zero, the first-guess field was left unchanged, and the analyzed value was simply the first-guess value. This correction procedure was applied at all grid points to produce an analyzed field. The resulting field was first smoothed with a median filter (Tukey, 1974; Rabiner *et al.,* 1975) and then smoothed with a five-point smoother of the type described by Shuman (1957) (hereafter referred as five-point Shuman smoother). The choice of first-guess fields is important and we discuss our procedures in section 3.2.5.

The analysis scheme is set up so that the

influence radius, and the number of five-point smoothing passes can be varied with each iteration. The strategy used is to begin the analysis with a large influence radius and decrease the radius with each iteration. This technique allows us to analyze progressively smaller size phenomena.

The analysis scheme is based on the work of several researchers analyzing meteorological data. Bergthorsson and Doos (1955) computed corrections to a first-guess field using various techniques: one assumed that the difference between a first-guess value and an analyzed value at a grid point was the same as the difference between an observation and a first-guess value at a nearby observing station. All the observed differences in an area surrounding the grid point were then averaged and added to the grid point first-guess value to produce an analyzed value. Cressman (1959) applied a distance-related weight function to each observation used in the correction in order to give more weight to observations that occur closest to the grid point. In addition, Cressman introduced the method of performing several iterations of the analysis scheme using the analysis produced in each iteration as the first-guess field for the next iteration. He also suggested starting the analysis with a relatively large influence radius and decreasing it with successive iterations to analyze smaller scale phenomena with each pass.

Sasaki (1960) introduced a weight function that was specifically related to the density of observations, and Barnes (1964, 1973) extended the work of Sasaki. The weight function of Barnes (1964) has been used here. The objective analysis scheme we used is commonly used by the mesoscale meteorological community.

Several studies of objective analysis techniques have been made. Achtemeier (1987) examined the "concept of varying influence radii for a successive corrections objective analysis scheme." Seaman (1983) compared the "objective analysis accuracies of statistical interpolation and successive correction schemes." Smith and Leslie (1984) performed an "error determination of a successive correction type objective analysis scheme." Smith *et al.* (1986) made "a comparison of errors in objectively analyzed fields for uniform and non-uniform station distribution." These are just a few examples of how various objective analysis techniques have been employed.

3.2.2. Derivation of Barnes (1964) weight function

The principle upon which the Barnes (1964) weight function is derived is that "the two-dimensional distribution of an atmospheric variable can be represented by the summation of an infinite number of independent harmonic waves, that is, by a Fourier integral representation". If $f(x,y)$ is the variable, then in polar coordinates (r,θ), a smoothed or filtered function $g(x,y)$ can be defined:

$$g(x,y) = \frac{1}{2\pi} \int_0^{2\pi} \int_0^\infty \eta f(x + r\cos\theta, y + r\sin\theta) d(\frac{r^2}{4K}) d\theta$$

(3)

in which r is the radial distance from a grid point whose coordinates are (x,y). The weight function is defined as

$$\eta = e^{-\frac{r^2}{4K}}$$

(4)

which resembles the Gaussian distribution. The shape of the weight function is determined by the value of K, which relates to the distribution of data. The weight function has the property that

$$\frac{1}{2\pi} \int_0^{2\pi} \int_0^\infty \eta d\left(\frac{r^2}{4K}\right) d\theta = 1$$

(5)

This property is desirable because in the continuous case (3) the application of the weight function to the distribution $f(x,y)$ will not change the mean of the distribution. However, in the discrete case (1), we only sum the contributions to within the distance R. This introduces an error in the evaluation of the filtered function, because the condition given by (5) does not apply. The error can be pre-determined and set to a reasonably small value in the following manner. If one carries out the integration in (5) with respect to θ, the remaining integral can be rewritten as

$$\int_0^R \eta d\left(\frac{r^2}{4K}\right) + \int_R^\infty \eta d\left(\frac{r^2}{4K}\right) = 1 \qquad (6)$$

Defining the second integral as ε yields

$$\int_0^R e^{-\frac{r^2}{4K}} d\left(\frac{r^2}{4K}\right) = 1 - \varepsilon \qquad (7)$$

Integrating (7), we obtain

$$\varepsilon = e^{-\frac{R^2}{4K}} \qquad (7a)$$

Taking the natural logarithm of both sides of (7a) leads to an expression for K,

$$K = R^2 / 4E \qquad (7b)$$

where $E \equiv$ -ln ε.

Rewriting (4) using (7b) leads to the form of weight function used in the evaluation of (1).

Thus, the choice of E and the specification of R determine the shape of the weight function.

Levitus (1982) chose $E=4$ which corresponds to a value of ε of approximately 0.02. This choice implies with respect to (7) the representation of more than 98 percent of the influence of any data around the grid point in the area defined by the influence radius R.

This analysis (WOA23) and previous analyses (WOA94, WOA98, WOA01, WOA05, WOA09, WOA13, and WOA18) used $E=4$.

Barnes (1964) proposed using this scheme in an iterative fashion similar to Cressman (1959). Levitus (1982) used a four-iteration scheme with a variable influence radius for each pass. As noted earlier, WOA94 used a one-iteration scheme, while WOA98, WOA01, WOA05, WOA09, WOA13, WOA18, and WOA23 employed a three-iteration scheme with a variable influence radius.

3.2.3. Derivation of Barnes (1964) response function

It is desirable to know the response of a data set to the interpolation procedure applied to it. Following Barnes (1964) and reducing to a one-dimensional case we let

$$f(x) = A \sin(\alpha x) \qquad (8)$$

in which $\alpha = 2\pi/\lambda$ with λ being the wavelength of a particular Fourier component, and substitute this function into equation (3) along with the expression for η in equation (4). Then

$$g(x) = D[A \sin(\alpha x)] = Df(x) \qquad (9)$$

in which D is the response function for one application of the analysis and defined as

$$D = e^{-\left(\frac{\alpha R}{4}\right)^2} = e^{-\left(\frac{\pi R}{2\lambda}\right)^2}.$$

The phase of each Fourier component is not changed by the interpolation procedure. The results of an analysis pass are used as the first-guess for the next analysis pass in an iterative fashion. The relationship between the filtered function $g(x)$ and the response function after N iterations as derived by Barnes (1964) is

$$g_N(x) = f(x)D\sum_{n=1}^{N}(1-D)^{n-1} \tag{10}$$

Equation (10) differs slightly from that given by Barnes. The difference is due to our first-guess field being defined as a zonal average, annual mean, seasonal mean, or monthly mean for "all-data" climatologies, whereas Barnes used the first application of the analysis as a first-guess. Barnes (1964) also showed that applying the analysis scheme in an iterative fashion will result in convergence of the analyzed field to the observed data field. However, it is not desirable to approach the observed data too closely, because at least seven or eight grid points are needed to represent a Fourier component.

The response function given in (10) is useful in two ways: it is informative to know what Fourier components make up the analyses, and the computer programs used in generating the analyses can be checked for correctness by comparison with (10).

3.2.4. Choice of response function

The distribution of salinity observations (see appendices) at different depths and for the different averaging periods, are not regular in space or time. At one extreme, regions exist in which every one-degree square contains data and no interpolation needs to be performed. At the other extreme are regions in which few if any data exist. Thus, with variable data spacing the average separation distance between grid points containing data is a function of geographical position and averaging period. However, if we computed and used a different average separation distance for each variable at each depth and each averaging period, we would be generating analyses in which the wavelengths of observed phenomena might differ from one depth level to another and from one season to another. In WOA94, a fixed influence radius of 555 kilometers was used to allow uniformity in the analysis of all variables. For WOA98, WOA01, WOA05, WOA09, WOA13, WOA18, and WOA23 analyses on the one-degree grid, a three-pass analysis based on Barnes (1964) with influence radii of 892, 669 and 446 km was used. For the WOA13, WOA18, and WOA23 analyses on the quarter-degree grid, a three-pass analysis with radii of influence of 321, 267, and 214 km was used. (See Table 1 in section *3.4.1* for a comparison of the radii of influences on the different grids.)

Inspection of (1) shows that the difference between the analyzed field and the first-guess field values at any grid point is proportional to the sum of the weighted-differences between the observed mean and first-guess at all grid points containing data within the influence area.

The reason for using the five-point Shuman smoother and the median smoother is that our data are not evenly distributed in space. As the analysis moves from regions containing data to regions devoid of data, small-scale discontinuities may develop. The five-point Shuman and median smoothers are used to help eliminate these discontinuities. The five-point Shuman smoother does not affect the phase of the Fourier components that comprise an analyzed field.

The response functions for the analyses presented in these atlases are given in Table 5 and Figure 1. For comparison purposes, the response function used by Levitus (1982), WOA94, and others are also presented. The response function represents the smoothing inherent in the objective analysis described above plus the effects of one application of the five-point Shuman smoother and one application of a five-point median smoother. The effect of varying the amount of smoothing in North Atlantic sea surface temperature (SST) fields has been quantified by Levitus (1982) for a particular case. In a region of strong SST gradient such as the Gulf Stream, the effect of smoothing can

easily be responsible for differences between analyses exceeding 1.0°C.

To avoid the problem of the influence region extending across land or sills to adjacent basins, the objective analysis routine employs basin "identifiers" to preclude the use of data from adjacent basins. Table 6 lists these basins and the depth at which no exchange of information between basins is allowed during the objective analysis of data, *i.e.* "depths of mutual exclusion." Some regions are nearly, but not completely, isolated topographically. Because some of these nearly isolated basins have water mass properties that are different from surrounding basins, we have chosen to treat these as isolated basins as well. Not all such basins have been identified because of the complicated structure of the sea floor. In Table 6, a region marked with an asterisk (*) can interact with adjacent basins except for special areas such as the Isthmus of Panama.

3.2.5. First-guess field determination

There are gaps in the data coverage and, in some parts of the world ocean, there exist adjacent basins whose water mass properties are individually nearly homogeneous but have distinct basin to basin differences. Spurious features can be created when an influence area extends over two basins of this nature (basins are listed in Table 6). Our choice of first-guess field attempts to minimize the creation of such features. To maximize data coverage and best represent global variability, a set of "time-indeterminant" climatologies were produced as a first-guess for each set of decadal climatologies. The time-indeterminant climatologies used the first-guess field procedures developed for earlier versions of WOA. To provide a first-guess field for the "all-data" annual analysis at any standard level, we first zonally averaged the observed salinity data in each one-degree latitude belt by individual ocean basins. The annual analysis was then used as the first-guess for each seasonal analysis and each seasonal analysis was used as a first-guess for the appropriate monthly analysis if computed.

We then reanalyzed the salinity data using the newly produced analyses as first-guess fields described as follows and as shown in Figure 2. A new annual mean was computed as the mean of the twelve monthly analyses for the upper 1500 m, and the mean of the four seasons below 1500 m depth. This new annual mean was used as the first-guess field for new seasonal analyses. These new seasonal analyses in turn were used to produce new monthly analyses. This procedure produces slightly smoother means.

These time-indeterminant monthly mean objectively analyzed salinity fields were used as the first-guess fields for each "decadal" monthly climatology. Likewise, time-indeterminant seasonal and annual climatologies were used as first-guess fields for the seasonal and annual decadal climatologies.

We recognize that fairly large data-void regions exist, in some cases to such an extent that a seasonal or monthly analysis in these regions is not meaningful. Geographic distribution of observations for the "all-data" annual periods (see appendices) is excellent for the upper layers of the ocean. By using an "all-data" annual mean, first-guess field regions where data exist for only one season or month will show no contribution to the annual cycle. By contrast, if we used a zonal average for each season or month, then, in those latitudes where gaps exist, the first-guess field would be heavily biased by the few data points that exist. If these were anomalous data in some way, an entire basin-wide belt might be affected.

One advantage of producing "global" fields for a particular compositing period (even though some regions are data void) is that such analyses can be modified by

investigators for use in modeling studies.

For the time-indeterminant quarter-degree first-guess field, the one-degree time-indeterminant field was also used. Each of the sixteen quarter-degree boxes enclosed used the one-degree time-indeterminant value as a first-guess, thereby projecting the one-degree climatology onto the quarter-degree grid. In those areas where there was no one-degree value due to land or bottom mask, the statistical mean for the entire basin at the given depth was used. This first-guess field was then used to calculate time-indeterminant quarter-degree field. The time indeterminant quarter-degree field was then used for each quarter-degree decadal climatological mean.

3.3. Choice of objective analysis procedures

Optimum interpolation (Gandin, 1963) has been used by some investigators to objectively analyze oceanographic data. Although we recognize the power of this technique we have not used it to produce analyzed fields. As described by Gandin (1963), optimum interpolation is used to analyze synoptic data using statistics based on historical data. In particular, the second-order statistics such as correlation functions are used to estimate the distribution of first order parameters such as means. We attempt to map most fields in this atlas based on relatively sparse data sets.

Because of the paucity of data, we prefer not to use an analysis scheme that is based on second order statistics. In addition, as Gandin (1963) has noted, there are two limiting cases associated with optimum interpolation. The first is when a data distribution is dense. In this case, the choice of interpolation scheme makes little difference. The second case is when data are sparse. In this case, an analysis scheme based on second order statistics is of questionable value. For additional information on objective analysis procedures see Thiebaux and Pedder (1987) and Daley (1991).

3.4. Choice of spatial grid

The analyses that comprise WOA23 have been computed using the ETOPO2 (Earth Topography 2 arc minute) land-sea topography to define ocean depths at each grid point (ETOPO2, 2006). From the ETOPO2 land mask, a quarter-degree land mask was created based on ocean bottom depth and land criteria. If sixteen or more 2-minute square values out of a possible forty-nine in a one-quarter-degree box were defined as land, then the quarter-degree grid box was defined to be land. If no more than two of the 2-minute squares had the same depth value in a quarter-degree box, then the average value of the 2-minute ocean depths in that box was defined to be the depth of the quarter-degree grid box. If ten or more 2-minute squares out of the forty-nine had a common bottom depth, then the depth of the quarter-degree box was set to the most common depth value. The same method was used to go from a quarter-degree to a one-degree resolution. In the one-degree resolution case, at least four points out of a possible sixteen (in a one-degree square) had to be land in order for the one-degree square to remain land and three out of sixteen had to have the same depth for the ocean depth to be set. These criteria yielded a mask that was then modified by:

1. Connecting the Isthmus of Panama;
2. Maintaining an opening in the Straits of Gibraltar and in the English Channel;
3. Connecting the Kamchatka Peninsula and the Baja Peninsula to their respective continents.

The one-degree mask was created from the quarter-degree mask instead of directly from ETOPO2 in order to maintain consistency

between the quarter-degree and one-degree masks.

3.4.1 Increased Spatial Resolution

Like its two predecessors (WOA13 and WOA18), WOA23 consists of temperature and salinity climatologies at both one-degree and quarter-degree spatial resolution. The increase in resolution from one-degree to quarter-degree between WOA09 and WOA13 allowed regions whose features were not clearly defined in the one-degree analysis to be better represented in the higher-resolution analysis. For example, the improved representation of the California Current from 1-degree to ¼-degree resolution in both WOA13 (Fig. 1 in Zweng *et al.*, 2013) and WOA18 (Fig. 1 in Zweng *et al.*, 2018) continues to be evident in WOA23. One reason for this improved representation in the higher spatial resolution climatology is due to the quarter-degree land grid boxes being closer and more confined to the coast than the one-degree land grid-boxes, whose land grid boxes extend much further into the ocean. This allows the quarter-degree WOA13, WOA18, and WOA23 to better use the large amount of data in near-shore observations.

Table 1. Radii of influence used in the objective analysis for the one-degree and quarter-degree climatologies.

Pass Number	1° Radius of Influence	1/4° Radius of Influence
1	892 km	321 km
2	669 km	267 km
3	446 km	214 km

However, some drawbacks are also encountered when moving to a higher resolution. The radius of influence used in the objective analysis is smaller in the quarter-degree grid as compared to the one-degree grid (see Table 1), thus in regions of very few observations, the analyzed value will not have many, if any, data points used in its calculation. This issue has been minimized somewhat by using the one-degree climatological products as first-guess fields for the quarter-degree products. For a full discussion of the methods used in producing the quarter-degree fields see Boyer *et al.* (2005).

3.5. Stabilization of Temperature and Salinity Climatologies

Temperature and salinity climatologies are calculated separately. There are many more temperature data than salinity data. Even when there are salinity measurements, there are not always concurrent temperature measurements. As a result, when density is calculated from standard level climatologies of temperature and salinity, instabilities may result in the vertical density field. (Stability is defined in section 2.2.4.) While instabilities do occur in the ocean on an instantaneous time frame, these instabilities are usually short-lived and not characteristic of the mean density field. Appendices A (Section 8.1) and B (Section 8.2) describe a method we have employed to minimally alter climatological temperature and salinity profiles to achieve a stable water column everywhere in the world ocean. The method is based on the technique of Jackett and McDougall (1995). The final temperature and salinity climatologies reflect this stabilization. Appendix C (Section 8.3) describes some areas where the salinity fields should be used with care due to data scarcity.

3.5.1 Adjusting large stabilization changes

After inspecting the WOA23 salinity (and temperature) fields post-stabilization, there were a few small regions that developed large salinity "bullseyes." These were isolated to the early decades and in regions that had very few observations. With very few observations, the data that did exist influenced a large area (as determined by the radius of influence). Additionally, many of these observations were taken from instruments (*e.g.,* MBT) that did not extend much past 200m so their influence was only

on the upper water column, with the remaining water column having no data and being primarily represented by the first guess field. This led to large inversions in some cases in the pre-stabilized fields.

Please see Appendix D (Section 8.4) for an example of where this occurred and how it was remedied. Additionally, all areas for which a fix was introduced to resolve this issue is provided.

4. RESULTS

The online figures for this atlas include eight types of horizontal maps (a-h below) representing annual, seasonal, and monthly spatial distributions of analyzed data and data statistics as a function of selected standard depth levels for salinity:

a) Objectively analyzed salinity climatology fields. One-degree or quarter-degree grids (as applicable) for which there were fewer than three values available in the objective analysis defined by the influence radius are denoted by a white "/" symbol.

b) Statistical mean salinity fields. One-degree or quarter-degree grids of statistical means (based on observed data within each grid box) used in the objective analysis.

c) Data distribution fields of the number of salinity observations in each one-degree or quarter-degree grid used in the objective analysis, binned into 1 to 2, 3-5, 6-10, 11-30, 31-50 and greater than 51 observations per grid square.

d) Standard deviation salinity fields binned into several ranges depending on the depth level. The maximum value of the standard deviation is shown on the map.

e) Objectively analyzed standard deviation salinity fields. *New WOA23 field.*

f) Standard error of the mean salinity fields binned into several ranges depending on the depth level.

g) Difference between observed and analyzed salinity fields binned into several ranges depending on the depth level.

h) Difference between seasonal/monthly salinity fields and the annual mean field.

i) The number of mean salinity values within the radius of influence for each grid box was also calculated. This is not represented as stand-alone online maps, but the results are used in a) and b) maps (as above) to shade the grid boxes with fewer than three mean values within the radius of influence. These calculations are available as data files online.

j) Standard error of the analysis. This field is also not part of the online figure suite, but is included in the data files. See Levitus *et al.* (2012) for a full description. *New WOA23 field.*

The maps are arranged by composite time periods: annual, seasonal, monthly. We note that the complete set of all climatological maps, objectively analyzed fields and associated statistical fields at all standard depth levels are shown in Table 2. The complete set of data files and documentation are available online. Table 7 describes all available salinity maps and data files.

All of the figures use consistent symbols and notations for displaying information. Continents are displayed as light-grey areas. Oceanic areas shallower than the standard depth level being displayed are shown as solid gray areas. The objectively analyzed distribution fields include the nominal contour interval used. In addition, these maps may include in some cases additional contour lines displayed as dashed black lines. All of the maps were computer-drafted using python programming language.

In the next sub-section, we describe the computation of annual and seasonal fields

(section 4.1) and available objective and statistical fields (section 4.2).

4.1. Computation of annual and seasonal fields

After completion of all of our analyses we define a final annual analysis as the average of our twelve monthly-mean fields in the upper 1500 m of the ocean. Below 1500 m depth we define an annual analysis as the mean of the four seasonal analyses. Our final seasonal analyses are defined as the average of the monthly analyses in the upper 1500 m of the ocean.

4.2. Available statistical fields

Table 7 lists all objective and statistical fields calculated as part of WOA23. Climatologies of salinity and associated statistics described in this document, as well as global figures of the same, can be obtained online.

The sample standard deviation in a grid box was computed using:

$$s = \sqrt{\frac{\sum_{n=1}^{N}(x_n - \overline{x})^2}{N-1}} \qquad (11)$$

in which x_n= the nth data value in the grid box, $\overline{x}$ = mean of all data values in the grid box, and N = total number of data values in the grid box. The standard error of the mean was computed by dividing the standard deviation by the square root of the number of observations in each grid box.

In addition to statistical fields, the land/ocean bottom mask and basin definition mask are also available on the above-mentioned website. A user could take the standard depth level data from WOD23 with flags and these masks, and recreate the WOA23 fields following the procedures outlined in this document. Explanations and data formats for the data files are found under documentation on the WOA23 webpage.

WOA23 salinity introduces two new ancillary fields. The first is the objectively analyzed standard deviation. These fields are computed using the same objective analysis discussed in section *3.2*, but the input values are the 1 or ¼-degree statistical standard deviations. We further refine the input standard deviations by only incorporating standard deviation grids in which there were at least six observations within that grid box. Since we eliminated all grid points that had less than six observations in the objective analysis of the standard deviations, it is important that these fields be used with much caution, particularly in early decades when data availability was much less than present time. It is highly recommended that when using the standard deviation objectively analyzed fields, that the user pays close attention to the data distribution field as well. The data distribution figures that are available online do contain a contour interval at 6 allowing for easy visualization of grid points that were included (and were not) in the objectively analyzed standard deviation fields.

The second field introduced in WOA23 salinity is the standard error of the analysis. This is one estimate of the uncertainty in the objective analysis. It is computed by calculating the standard error of the differences between the objectively analyzed and statistical mean fields [(j) in section *4*)] within the 2nd radius of influence (669 km for 1-degree, 267 km for ¼-degree). A full description of this field and its calculation can be found in the supplement of Levitus *et al.* (2012).

4.3 Obtaining WOA23 fields online

The objective and statistical data fields can be obtained online in different digital formats at the WOA23 webpage. The WOA23 fields can be obtained in ASCII format (WOA native and comma-separated value [CSV]), ArcGIS compatible format, and netCDF

through our WOA23 webpage. WOA23 includes a digital collection of "PNG" images of the objective and statistical fields. In addition, WOA23 can be obtained in Ocean Data View (ODV) format. WOA23 will be available through other online locations as well. WOA98, WOA01, WOA05, WOA09 are presently served through the IRI/LDEO Climate Data Library with access to statistical and objectively analyzed fields in a variety of digital formats.

5. SUMMARY

We have described the results of a project to objectively analyze all historical ocean salinity data in WOD23. The goal was to build a set of climatological analyses that are identical in all respects for all variables including relatively data sparse variables such as nutrients. This provides investigators with a consistent set of analyses to use.

One advantage of the analysis techniques used in this atlas is that we know the amount of smoothing by the objective analyses is given by the response function in Table 5 and Figure 1. This is an important function for constructing and describing a climatology of any geophysical parameter. Particularly, when computing anomalies from a standard climatology, it is important that the synoptic field be smoothed to the same extent as the climatology in order to prevent the generation of spurious anomalies simply through differences in smoothing. A second reason is that purely diagnostic computations require a minimum of seven or eight grid points to represent any Fourier component with accuracy. Higher order derivatives will require more smoothing.

We have attempted to create objectively analyzed fields and data sets that can be used as a "black box." We emphasize that some quality control procedures used are subjective. For those users who wish to make their own choices, all the data used in our

analyses are available both at standard depth levels as well as observed depth levels. The results presented in this atlas show some features that are suspect and may be due to non-representative data that were not flagged by the quality control techniques used. Although we have attempted to eliminate as many of these features as possible by flagging the data which generate these features, some of these features may remain. It should be noted that some of these flagged data may eventually turn out not to be artifacts but rather do represent real features, not yet capable of being described in a meaningful way due to lack of data.

6. FUTURE WORK

Our analyses will be updated when justified by additional observations. As more data are received at NCEI/WDS, we will also be able to produce improved higher resolution climatologies for salinity.

We recognize that our statistical flagging of standard level data assumes that the data within each 5-degree box is normally distributed. This assumption fails in certain regions of the ocean. Therefore, we are currently investigating alternative methods for quality control flagging. These include alternative statistics that do not require Gaussian distributions, and leveraging machine learning to better cluster the data before applying statistical checks.

Finally, there are still certain regions of the global ocean that are severely under sampled (*e.g.,* Arctic Ocean in boreal winter) and thus large uncertainties continue to remain in the climatologies for these regions. Future work will also be investigating better methods to help quantify the uncertainties in these regions. WOA23 takes a step forward in this regard by providing standard error of the analysis fields, but additional sources of uncertainty remain and need to be better

quantified.

7. REFERENCES

Achtemeier, G.L. (1987). On the concept of varying influence radii for a successive corrections objective analysis. *Mon. Wea. Rev.,* 11, 1761-1771.

Antonov, J.I., S. Levitus, T.P. Boyer, M.E. Conkright, T.D. O'Brien, and C. Stephens (1998a). World Ocean Atlas 1998. Vol. 1: Temperature of the Atlantic Ocean*. NOAA Atlas NESDIS 27*, U.S. Government Printing Office, Washington, D.C., 166 pp.

Antonov, J.I., S. Levitus, T.P. Boyer, M.E. Conkright, T.D. O'Brien, and C. Stephens (1998b). World Ocean Atlas 1998. Vol. 2: Temperature of the Pacific Ocean. *NOAA Atlas NESDIS 28*, U.S. Government Printing Office, Washington, D.C., 166 pp.

Antonov, J.I., S. Levitus, T.P. Boyer, M.E. Conkright, T.D. O'Brien, C. Stephens, and B. Trotsenko (1998c). World Ocean Atlas 1998. Vol. 3: Temperature of the Indian Ocean. *NOAA Atlas NESDIS 29*, U.S. Government Printing Office, Washington, D.C., 166 pp.

Antonov, J.I., R.A. Locarnini, T.P. Boyer, H.E. Garcia, and A.V. Mishonov (2006). World Ocean Atlas 2005. Vol. 2: Salinity. S. Levitus, Ed. *NOAA Atlas NESDIS 62*, U.S. Government Printing Office, Washington, D.C., 182 pp.

Antonov, J.I., D. Seidov, T.P. Boyer, R.A. Locarnini, A.V. Mishonov, H.E. Garcia, O.K. Baranova, M.M. Zweng, and D.R. Johnson (2010). World Ocean Atlas 2009. Vol. 2: Salinity. S. Levitus, Ed. *NOAA Atlas NESDIS 69*, U.S. Government Printing Office, Washington, D.C., 184 pp.

Argo (2000). Argo float data and metadata from Global Data Assembly Centre (Argo GDAC). SEANOE. https://doi.org/10.17882/42182

Barnes, S.L. (1964). A technique for maximizing details in numerical weather map analysis. *J. App. Meteor.*, 3, 396-409.

Barnes, S.L. (1973). Mesoscale objective map analysis using weighted time series observations*. NOAA Technical Memorandum ERL* NSSL-62, 60 pp.

Barnes, S.L. (1994). Applications of the Barnes Objective Analysis Scheme, Part III: Tuning for Minimum Error. *J. Atmos. Oceanic Technol.,* 11, 1459-1479.

Bergthorsson, P. and B. Doos, (1955). Numerical Weather map analysis. *Tellus*, 7, 329-340.

Boyer, T.P. and S. Levitus (1994). Quality control and processing of historical temperature, salinity and oxygen data. *NOAA Technical Report NESDIS 81*, 65 pp.

Boyer, T.P., S. Levitus, J.I. Antonov, M.E. Conkright, T.D. O'Brien, and C. Stephens (1998a). World Ocean Atlas 1998. Vol. 4: Salinity of the Atlantic Ocean. *NOAA Atlas NESDIS* 30, U.S. Government Printing Office, Washington, D.C., 166 pp.

Boyer, T.P., S. Levitus, J.I. Antonov, M.E. Conkright, T.D. O'Brien, and C. Stephens (1998b). World Ocean Atlas 1998. Vol. 5: Salinity of the Pacific Ocean. *NOAA Atlas NESDIS 31*, U.S. Government Printing Office, Washington, D.C., 166 pp.

Boyer, T.P., S. Levitus, J.I. Antonov, M.E. Conkright, T.D. O'Brien, C. Stephens, and B. Trotsenko (1998c). World Ocean Atlas 1998. Vol. 6: Salinity of the Indian Ocean. *NOAA Atlas NESDIS 32*, U.S. Government Printing Office, Washington, D.C., 166 pp.

Boyer, T.P., C. Stephens, J.I. Antonov, M.E. Conkright, R.A. Locarnini, T.D. O'Brien, and H.E. Garcia (2002). World Ocean Atlas 2001. Vol. 2: Salinity. S. Levitus, Ed., *NOAA Atlas NESDIS 50*, U.S. Government Printing Office, Washington, D.C., 165 pp.

Boyer, T.P, S. Levitus, H.E. Garcia, R.A. Locarnini, C. Stephens, J.I. Antonov (2005). Objective analyses of annual, seasonal, and monthly temperature and salinity for the world ocean on a ¼ degree grid. *International Journal of Climatology*, 25, 931-945.

Boyer, T.P., R.A. Locarnini, M.M. Zweng, A.V. Mishonov, J.R. Reagan, J.I. Antonov, H.E. Garcia, O.K. Baranova, D.R. Johnson, D. Seidov, M.M. Biddle, M. Hamilton (2015). *Changes to calculations of the World Ocean Atlas 2013 for ver.2*. http://data.nodc.noaa.gov/woa/WOA13/DOC/woa13v2_changes.pdf

Boyer, T.P., O.K. Baranova, C. Coleman, H.E. Garcia, A. Grodsky, R.A. Locarnini, A.V. Mishonov, C.R. Paver, J.R. Reagan, D. Seidov, I.V. Smolyar, K.W. Weathers, M.M. Zweng (2019). World Ocean Database 2018. A. V. Mishonov, Tech. Editor, *NOAA Atlas NESDIS 87*.

Conkright, M.E., S. Levitus, and T.P. Boyer (1994). World Ocean Atlas 1994. Vol. 1: Nutrients.

19

NOAA Atlas NESDIS 1, U.S. Government Printing Office, Washington, D.C., 150 pp.

Conkright, M.E., T.D. O'Brien, S. Levitus, T.P. Boyer, J.I. Antonov, and C. Stephens (1998a). World Ocean Atlas 1998. Vol. 10: Nutrients and Chlorophyll of the Atlantic Ocean. *NOAA Atlas NESDIS 36*, U.S. Government Printing Office, Washington, D.C., 245 pp.

Conkright, M.E., T.D. O'Brien, S. Levitus, T.P. Boyer, J.I. Antonov, and C. Stephens (1998b). World Ocean Atlas 1998. Vol. 11: Nutrients and Chlorophyll of the Pacific Ocean. *NOAA Atlas NESDIS 37*, U.S. Government Printing Office, Washington, D.C., 245 pp.

Conkright, M.E., T.D. O'Brien, S. Levitus, T.P. Boyer, J.I. Antonov, and C. Stephens (1998c). World Ocean Atlas 1998. Vol. 12: Nutrients and Chlorophyll of the Indian Ocean. *NOAA Atlas NESDIS 38*, U.S. Government Printing Office, Washington, D.C., 245 pp.

Conkright, M.E., H.E. Garcia, T.D. O'Brien, R.A. Locarnini, T.P. Boyer, C. Stephens, and J.I. Antonov (2002*).* World Ocean Atlas 2001. Vol. 4: Nutrients. S. Levitus, Ed., *NOAA Atlas NESDIS 52*, U.S. Government Printing Office, Washington, D.C., 392 pp.

Cressman, G.P. (1959). An operational objective analysis scheme. *Mon. Wea. Rev.*, 87, 329-340.

Daley, R. (1991). *Atmospheric Data Analysis.* Cambridge University Press, Cambridge, 457 pp.

ETOPO2 (2006). Data Announcements 06-MGG-01, 2-Minute Gridded Global Relief Data. NOAA, *National Geophysical Data Center*, Boulder, CO.

Gandin, L.S. (1963). Objective Analysis of Meteorological fields. *Gidromet Izdat*, Leningrad (translation by Israel program for Scientific Translations), Jerusalem, 1966, 242 pp.

Garcia, H.E., R.A. Locarnini, T.P. Boyer, and J.I. Antonov (2006a). World Ocean Atlas 2005. Vol. 3: Dissolved Oxygen, Apparent Oxygen Utilization, and Oxygen Saturation. S. Levitus, Ed. *NOAA Atlas NESDIS 63*, U.S. Government Printing Office, Washington, D.C., 342 pp.

Garcia H.E., R.A. Locarnini, T.P. Boyer, and J.I. Antonov (2006b). World Ocean Atlas 2005. Vol. 4: Nutrients (phosphate, nitrate, silicate), S. Levitus, Ed., *NOAA Atlas NESDIS 64*, U.S. Government Printing Office, Washington, D.C., 395 pp.

Garcia, H.E., R.A. Locarnini, T.P. Boyer, and J.I. Antonov (2010a). World Ocean Atlas 2009, Vol. 3: Dissolved Oxygen, Apparent Oxygen Utilization, and Oxygen Saturation. S. Levitus, Ed. *NOAA Atlas NESDIS 70*, U.S. Government Printing Office, Washington, D.C., 344 pp.

Garcia, H.E., R.A. Locarnini, T.P. Boyer, and J.I. Antonov (2010b). World Ocean Atlas 2009. *I* S. Levitus, Ed. *NOAA Atlas NESDIS 71*, U.S. Government Printing Office, Washington, D.C., 398 pp.

Garcia, H. E., R. A. Locarnini, T. P. Boyer, J. I. Antonov, O.K. Baranova, M.M. Zweng, J.R. Reagan, D.R. Johnson (2013a). *World Ocean Atlas 2013, Volume 3: Dissolved Oxygen, Apparent Oxygen Utilization, and Oxygen Saturation.* S. Levitus, Ed., A. Mishonov Tech. Ed.; *NOAA Atlas NESDIS 75*, 27 pp.

Garcia, H. E., R. A. Locarnini, T. P. Boyer, J. I. Antonov, O.K. Baranova, M.M. Zweng, J.R. Reagan, D.R. Johnson (2013b). *World Ocean Atlas 2013, Volume 4: Dissolved Inorganic Nutrients (phosphate, nitrate, silicate).* S. Levitus, Ed., A. Mishonov Tech. Ed.; *NOAA Atlas NESDIS 76*, 25 pp.

Garcia H.E., K.W. Weathers, C.R. Paver, I.V. Smolyar, T.P. Boyer, R.A. Locarnini, M.M. Zweng, A.V. Mishonov, O.K. Baranova, and J.R. Reagan (2019a). World Ocean Atlas 2018, Vol. 3: Dissolved Oxygen, Apparent Oxygen Utilization, and Oxygen Saturation. A. Mishonov, Tech. Ed. *NOAA Atlas NESDIS 83*, 29pp.

Garcia H.E., K.W. Weathers, C.R. Paver, I.V. Smolyar, T.P. Boyer, R.A. Locarnini, M.M. Zweng, A.V. Mishonov, O.K. Baranova, and J.R. Reagan (2019b). World Ocean Atlas 2018, Vol. 4: Dissolved Inorganic Nutrients (phosphate, nitrate, silicate). A. Mishonov, Tech. Ed. *NOAA Atlas NESDIS 84*, 34pp.

Garcia, H.E., Z. Wang, C. Bouchard, S.L. Cross, C.R. Paver, J.R. Reagan, T.P. Boyer, R.A. Locarnini, A.V. Mishonov, O. Baranova, D. Seidov, and D. Dukhovskoy (2024a). World Ocean Atlas 2023, Vol. 3: Dissolved Oxygen, Apparent Oxygen Utilization, and Oxygen Saturation. A. Mishonov, Tech. Ed. *NOAA Atlas NESDIS 91*, 100 pp, https://doi.org/10.25923/rb67-ns53.

Garcia, H.E., C. Bouchard, S.L. Cross, C.R. Paver, Z. Wang, J.R. Reagan, T.P. Boyer, R.A. Locarnini, A.V. Mishonov, O. Baranova, D. Seidov, and D. Dukhovskoy (2024b). World Ocean Atlas 2023, Vol. 4: Dissolved Inorganic Nutrients (phosphate, nitrate, silicate). A. Mishonov, Tech. Ed. *NOAA Atlas NESDIS 92*, 34pp, https://doi.org/10.25923/39qw-7j08

Garcia, H. E., T. P. Boyer, R. A. Locarnini, J.R. Reagan, A.V. Mishonov, O.K. Baranova, C.R. Paver (2024c). World Ocean Database 2023: User's Manual. A.V. Mishonov, Tech. Ed., *NOAA Atlas NESDIS 98,* pp 114 https://doi.org/10.25923/j8gq-ee82 (in preparation).

Hesselberg, T. and H.U. Sverdrup (1914). Die Stabilitutsverhaltnisse des Seewassers bei Vertitalen Verschiebungen. *Aarb. Bergen Mus.,* No. 14, 17 pp.

IOC (1998). Global Temperature-Salinity Profile Programme (GTSPP) – Overview and Future. *IOC Technical Series, 49*, Intergovernmental Oceanographic Commission, Paris, 12 pp.

Jackett, D.R. and T.J. McDougall (1995). Minimal Adjustment of Hydrographic Profiles to Achieve Static Stability. *J. Atmos. Oceanic Technol.*, 12, 381-389.

JPOTS (Joint Panel on Oceanographic Tables and Standards) Editorial Panel (1991). Processing of Oceanographic Station Data. *UNESCO*, Paris, 138 pp.

Johnson, G.C. (1995). Revised XCTD fall-rate equation coefficients from CTD data. *J. Atmos. Oceanic Technol.*, 12, 1367-1373.

Kizu, S., H. Onishi, T. Suga, K. Hanawa, T. Watanabe, and H. Iwamiya (2008). Evaluation of the fall rates of the present and developmental XCTDs. *Deep-Sea Res. I*, 55,571–586.

Koso, Y., H. Ishii, and M. Fujita (2005). An examination of the depth conversion formula of XCTD-2F. *Technical Bulletin on Hydrology and Oceanography*, 23, 93–98 (in Japanese).

Levitus, S. (1982). Climatological Atlas of the World Ocean. *NOAA Professional Paper No. 13*, U.S. Government Printing Office, Washington, D.C., 173 pp.

Levitus, S. and G. Isayev (1992). A polynomial approximation to the International Equation of State for Seawater. *J. Atmos. Oceanic Technol.,* 9, 705-708.

Levitus, S. and T.P. Boyer (1994a). World Ocean Atlas 1994. Vol. 2: Oxygen. *NOAA Atlas NESDIS 2*, U.S. Government Printing Office, Washington, D.C., 186 pp.

Levitus, S. and T.P. Boyer (1994b). World Ocean Atlas 1994. Vol. 4: Temperature. *NOAA Atlas NESDIS 4*, U.S. Government Printing Office, Wash., D.C., 117 pp.

Levitus, S., R. Burgett, T.P. Boyer (1994c). World Ocean Atlas 1994, Vol. 3: Salinity. *NOAA Atlas NESDIS 3*, U.S. Government Printing Office, Washington, D.C., 99 pp.

Levitus, S., S. Sato, C. Maillard, N. Mikhailov, P. Caldwell, and H. Dooley (2005). Building Ocean Profile-Plankton Databases for Climate and Ecosystem Research, *NOAA Technical Report NESDIS 117*, U.S Government Printing Office, Washington, D.C., 29 pp.

Levitus, S., et al. (2012). World ocean heat content and thermosteric sea level change (0–2000 m), 1955–2010, *Geophys. Res. Lett.*, 39, L10603, doi:10.1029/2012GL051106

Locarnini, R.A., T.D. O'Brien, H.E. Garcia, J.I. Antonov, T.P. Boyer, M.E. Conkright, and C. Stephens (2002). World Ocean Atlas 2001. Vol. 3: Oxygen. S. Levitus, Ed., *NOAA Atlas NESDIS 51*, U.S. Government Printing Office, Washington, D.C., 286 pp.

Locarnini, R.A., A.V. Mishonov, J.I. Antonov, T.P. Boyer, and H.E. Garcia (2006). World Ocean Atlas 2005. Vol. 1: Temperature. S. Levitus, Ed., NOAA *Atlas NESDIS 61*, U.S. Government Printing Office, Washington, D.C. 182 pp.

Locarnini, R.A., A.V. Mishonov, J.I. Antonov, T.P. Boyer, and H.E. Garcia (2010). World Ocean Atlas 2009. Vol. 1: Temperature. S. Levitus, Ed. *NOAA Atlas NESDIS 68*, U.S. Government Printing Office, Washington, D.C., 184 pp.

Locarnini, R.A., A.V. Mishonov, J.I. Antonov, T.P. Boyer, H.E. Garcia, O.K. Baranova, M.M. Zweng, C.R. Paver, J.R. Reagan, D.R. Johnson, M. Hamilton, D. Seidov (2013). World Ocean Atlas 2013, Vol. 1: Temperature. S. Levitus, Ed. A. Mishonov, Tech. Ed. *NOAA Atlas NESDIS 73*, 40 pp.

Locarnini, R.A., A.V. Mishonov, O.K. Baranova, T.P. Boyer, J.R. Reagan, H.E. Garcia, J.R. Reagan, D. Seidov, K. Weathers, C.R. Paver, I. Smolyar (2019). World Ocean Atlas 2018, Volume 1: Temperature. A. Mishonov Tech. Ed. *NOAA Atlas NESDIS 81*, 52 pp.

Locarnini, R.A., A.V. Mishonov, O.K. Baranova, J.R. Reagan, T.P. Boyer, D. Seidov, Z. Wang, H.E. Garcia, C. Bouchard, S.L. Cross, C.R. Paver, and D. Dukhovskoy (2024a). World Ocean Atlas 2023, Volume 1: Temperature. A. Mishonov Tech. Ed. *NOAA Atlas NESDIS 89*, 51 pp, https://doi.org/10.25923/54bh-1613

Locarnini, R.A., A.V. Mishonov, O.K. Baranova, J.R. Reagan, T.P. Boyer, D. Seidov, Z. Wang, H.E. Garcia, C. Bouchard, S.L. Cross, C.R. Paver, and D. Dukhovskoy (2024b). World Ocean Atlas 2023, Volume 5: Density. A.

Mishonov Tech. Ed. *NOAA Atlas NESDIS 93*, https://doi.org/10.25923/mcn4-d695

Lynn, R.J. and J.L. Reid (1968). Characteristics and circulation of deep and abyssal waters. *Deep-Sea Res.*, 15, 577-598.

Mishonov, A.V., T.P. Boyer, O.K. Baranova, C.N. Bouchard, S.L. Cross, H.E. Garcia, R.A. Locarnini, C.R. Paver, J.R. Reagan, Z. Wang, D. Seidov, A.I. Grodsky, J. Beauchamp (2024a). World Ocean Database 2023. C. Bouchard, Technical Ed. *NOAA Atlas NESDIS 97*, DOI https://doi.org/10.25923/z885-h264 (in preparation).

Mishonov, A.V., R.A. Locarnini, O.K. Baranova, J.R. Reagan, T.P. Boyer, D. Seidov, Z. Wang, H.E. Garcia, C. Bouchard, S.L. Cross, C.R. Paver, and D. Dukhovskoy (2024b). World Ocean Atlas 2023, Volume 8: Bottom Temperature. J.R. Reagan Tech. Ed. *NOAA Atlas NESDIS 96*, https://doi.org/10.25923/s47b-gm86 (in preparation).

Mizuno, K. and T. Watanabe (1998). Preliminary results of in-situ XCTD/CTD comparison test. *J. Oceanogr.*, 54(4), 373-380.

Neumann, G. and W.J. Pierson (1966). Principles of Physical Oceanography. *Prentice Hall Inc.*, Englewood Cliffs, N.J., 545 pp.

O'Brien, T.D., S. Levitus, T.P. Boyer, M.E. Conkright, J.I. Antonov, and C. Stephens (1998a). World Ocean Atlas 1998. Vol. 7: Oxygen of the Atlantic Ocean. *NOAA Atlas NESDIS 33*, U.S. Government Printing Office, Washington, D.C., 234 pp.

O'Brien, T.D., S. Levitus, T.P. Boyer, M.E. Conkright, J.I. Antonov, and C. Stephens (1998b). World Ocean Atlas 1998. Vol. 8: Oxygen of the Pacific Ocean. *NOAA Atlas NESDIS 34*, U.S. Government Printing Office, Washington, D.C., pp.

O'Brien, T.D., S. Levitus, T.P. Boyer, M.E. Conkright, J.I. Antonov, and C. Stephens (1998c). World Ocean Atlas 1998. Vol. 9: Oxygen of the Indian Ocean. *NOAA Atlas NESDIS 35*, U.S. Government Printing Office, Washington, D.C., 234 pp.

Rabiner, L.R., M.R. Sambur, and C.E. Schmidt (1975). Applications of a nonlinear smoothing algorithm to speech processing, *IEEE Trans. on Acoustics, Speech and Signal Processing*, 23, 552-557.

Reagan, J.R., D. Seidov, Z. Wang, T.P. Boyer, R.A. Locarnini, O.K. Baranova, A.V. Mishonov, H.E. Garcia, C. Bouchard, S.L. Cross, C.R. Paver, and

D. Dukhovskoy (2024a). World Ocean Atlas 2023, Volume 6: Conductivity. A. Mishonov Tech. Ed. *NOAA Atlas NESDIS 94*, https://doi.org/10.25923/wz4d-6x65

Reiniger, R.F. and C.F. Ross (1968). A method of interpolation with application to oceanographic data. *Deep-Sea Res.*, 9, 185-193.

Sasaki, Y. (1960). An objective analysis for determining initial conditions for the primitive equations. Ref. 60-1 6T, Atmospheric Research Lab., *Univ. of Oklahoma Research Institute*, Norman, 23 pp.

Seaman, R.S. (1983). Objective Analysis accuracies of statistical interpolation and successive correction schemes. *Australian Meteor. Mag.*, 31, 225-240.

Seidov, D., A. Mishonov, J. Reagan, O. Baranova, S. Cross, and R. Parsons (2018). Regional climatology of the Northwest Atlantic Ocean—high-resolution mapping of ocean structure and change, *Bulletin of the American Meteorological Society*, 9(10), doi:10.1175/BAMS-D-17-0205.1

Shuman, F.G. (1957). Numerical methods in weather prediction: II. Smoothing and filtering. *Mon. Wea. Rev.*, 85, 357-361.

Smith, D.R., and F. Leslie (1984). Error determination of a successive correction type objective analysis scheme. *J. Atmos. Oceanic Technol.*, 1, 121-130.

Smith, D.R., M.E. Pumphry, and J.T. Snow (1986). A comparison of errors in objectively analyzed fields for uniform and nonuniform station distribution, *J. Atmos. Oceanic Technol.*, 3, 84-97.

Stephens, C., J.I. Antonov, T.P. Boyer, M.E. Conkright, R.A. Locarnini, T.D. O'Brien, H.E. Garcia (2002). World Ocean Atlas 2001. Vol. 1: Temperature. S. Levitus, Ed., *NOAA Atlas NESDIS 49*, U.S. Government Printing Office, Washington, D.C., 167 pp.

Sverdrup, H.U., M.W. Johnson, and R.H. Fleming (1942). The Oceans: Their physics, chemistry, and general biology. *Prentice Hall*, 1060 pp.

Thiebaux, H.J. and M.A. Pedder (1987). Spatial Objective Analysis: with applications in atmospheric science. *Academic Press*, 299 pp.

Tukey, J.W. (1974). Nonlinear (nonsuperposable) methods for smoothing data, in *"Cong. Rec."*, 1974 *EASCON*, 673 pp.

Wang, Z., J.R. Reagan, T.P. Boyer, R.A. Locarnini, O.K. Baranova, A.V. Mishonov, D. Seidov, H.E. Garcia, C. Bouchard, S.L. Cross, C.R. Paver, and D. Dukhovskoy (2024b). World Ocean Atlas

2023, Volume 7: Mixed Layer Depth. A. Mishonov Tech. Ed. *NOAA Atlas NESDIS 95*, 52 pp, https://doi.org/10.25923/4adh-kq71

Wessel, P. and W.H.F. Smith (1998). New, improved version of Generic Mapping Tools released, *EOS Trans. Amer. Geophys. U.*, 79, 579.

WMO Guidelines on the calculation of Climate Normals (2017). WMO-No. 1203.

Wong, A. P., *et al.* (2020). Argo data 1999–2019: Two million temperature-salinity profiles and subsurface velocity observations from a global array of profiling floats, Front. Marine Sci., 7, 700, https://doi.org/10.3389/fmars.2020.00700

Wong, A., Keeley, R., Carval, T., and Argo Data Management Team (2022). Argo Quality Control Manual for CTD and Trajectory Data, Ifremer, Brest, https://doi.org/10.13155/33951/

Wong, A. P. S., Gilson, J., and Cabanes, C. (2023). Argo salinity: bias and uncertainty evaluation, Earth Syst. Sci. Data, 15, 383–393, https://doi.org/10.5194/essd-15-383-2023

Zweng, M.M, J.R. Reagan, J.I. Antonov, R.A. Locarnini, A.V. Mishonov, T.P. Boyer, H.E. Garcia, O.K. Baranova, D.R. Johnson, D.Seidov, M.M. Biddle (2013). *World Ocean Atlas 2013, Volume 2: Salinity.* S. Levitus, Ed., A. Mishonov Tech. Ed.; NOAA Atlas NESDIS 74, 39 pp.

Zweng, M. M., J. R. Reagan, D. Seidov, T. P. Boyer, R. A. Locarnini, H. E. Garcia, A. V. Mishonov, O. K. Baranova, K. Weathers, C. R. Paver, and I. Smolyar (2019). World Ocean Atlas 2018, Volume 2: Salinity. A. Mishonov Tech. Ed.; NOAA Atlas NESDIS 82, 50pp.

Table 2. Descriptions of climatologies for salinity. The standard depth levels are shown in Table 4.

Depths for annual climatology	Depths for seasonal climatology	Depths for monthly climatology	Datasets used to calculate climatology
0-5500 meters (102 levels)	0-5500 meters (102 levels)	0-1500 meters (57 levels)	OSD, CTD, MRB, PFL, DRB, UOR, SUR, GLD

Table 3. Descriptions of datasets in WOD23.

OSD	Bottle, low-resolution Conductivity-Temperature-Depth (CTD), low-resolution XCTD data, and plankton data
CTD	High-resolution Conductivity-Temperature-Depth (CTD) data and high-resolution XCTD data
MBT	Mechanical BathyThermograph (MBT) data, DBT, micro-BT
XBT	eXpendable BathyThermograph (XBT) data
SUR	Surface only data (bucket, thermosalinograph)
APB	Autonomous Pinniped Bathythermograph - Time-Temperature-Depth recorders attached to elephant seals
MRB	Moored buoy data from TAO (Tropical Atmosphere-Ocean), PIRATA (moored array in the tropical Atlantic), TRITON (Japan-JAMSTEC), RAMA (moored array in the tropical Indian) and individual (usually coastal) buoys.
PFL	Profiling float data
DRB	Drifting buoy data from surface drifting buoys with thermistor chains
UOR	Undulating Oceanographic Recorder data from a Conductivity/Temperature/Depth probe mounted on a towed undulating vehicle
GLD	Glider data

Table 4. Acceptable distances (m) for defining interior (A) and exterior (B) values used in the Reiniger-Ross scheme for interpolating observed level data to standard levels.

Standard Level #	Standard Depths (m)	A	B	Standard Level #	Standard Depths (m)	A	B
1	0	50	200	52	1250	200	400
2	5	50	200	53	1300	200	1000
3	10	50	200	54	1350	200	1000
4	15	50	200	55	1400	200	1000
5	20	50	200	56	1450	200	1000
6	25	50	200	57	1500	200	1000
7	30	50	200	58	1550	200	1000
8	35	50	200	59	1600	200	1000
9	40	50	200	60	1650	200	1000
10	45	50	200	61	1700	200	1000
11	50	50	200	62	1750	200	1000
12	55	50	200	63	1800	200	1000
13	60	50	200	64	1850	200	1000
14	65	50	200	65	1900	200	1000
15	70	50	200	66	1950	200	1000
16	75	50	200	67	2000	1000	1000
17	80	50	200	68	2100	1000	1000
18	85	50	200	69	2200	1000	1000
19	90	50	200	70	2300	1000	1000
20	95	50	200	71	2400	1000	1000
21	100	50	200	72	2500	1000	1000
22	125	50	200	73	2600	1000	1000
23	150	50	200	74	2700	1000	1000
24	175	50	200	75	2800	1000	1000
25	200	50	200	76	2900	1000	1000
26	225	50	200	77	3000	1000	1000
27	250	100	200	78	3100	1000	1000
28	275	100	200	79	3200	1000	1000
29	300	100	200	80	3300	1000	1000
30	325	100	200	81	3400	1000	1000
31	350	100	200	82	3500	1000	1000
32	375	100	200	83	3600	1000	1000
33	400	100	200	84	3700	1000	1000
34	425	100	200	85	3800	1000	1000
35	450	100	200	86	3900	1000	1000
36	475	100	200	87	4000	1000	1000
37	500	100	400	88	4100	1000	1000
38	550	100	400	89	4200	1000	1000
39	600	100	400	90	4300	1000	1000
40	650	100	400	91	4400	1000	1000
41	700	100	400	92	4500	1000	1000
42	750	100	400	93	4600	1000	1000
43	800	100	400	94	4700	1000	1000
44	850	100	400	95	4800	1000	1000
45	900	200	400	96	4900	1000	1000
46	950	200	400	97	5000	1000	1000
47	1000	200	400	98	5100	1000	1000
48	1050	200	400	99	5200	1000	1000
49	1100	200	400	100	5300	1000	1000
50	1150	200	400	101	5400	1000	1000
51	1200	200	400	102	5500	1000	1000

Table 5. Response function of the objective analysis scheme as a function of wavelength for WOA23 and earlier analyses. Response function is normalized to 1.0.

Wavelength[1]	Levitus (1982)	WOA94	WOA98, '01, '05, '09, '13 One-degree	WOA13, '18, '23 Quarter-degree
360ΔX	1.000	0.999	1.000	1.000
180ΔX	1.000	0.997	0.999	1.000
120ΔX	1.000	0.994	0.999	0.999
90ΔX	1.000	0.989	0.998	0.999
72ΔX	1.000	0.983	0.997	0.998
60ΔX	1.000	0.976	0.995	0.997
45ΔX	1.000	0.957	0.992	0.996
40ΔX	0.999	0.946	0.990	0.994
36ΔX	0.999	0.934	0.987	0.993
30ΔX	0.996	0.907	0.981	0.990
24ΔX	0.983	0.857	0.969	0.984
20ΔX	0.955	0.801	0.952	0.978
18ΔX	0.923	0.759	0.937	0.972
15ΔX	0.828	0.671	0.898	0.960
12ΔX	0.626	0.532	0.813	0.939
10ΔX	0.417	0.397	0.698	0.913
9ΔX	0.299	0.315	0.611	0.894
8ΔX	0.186	0.226	0.500	0.868
6ΔX	3.75×10^{-2}	0.059	0.229	0.777
5ΔX	1.34×10^{-2}	0.019	0.105	0.695
4ΔX	1.32×10^{-3}	2.23×10^{-3}	2.75×10^{-2}	0.567
3ΔX	2.51×10^{-3}	1.90×10^{-4}	5.41×10^{-3}	0.364
2ΔX	5.61×10^{-7}	5.30×10^{-7}	1.36×10^{-6}	0.103
1ΔX	N/A	N/A	N/A	1.13×10^{-4}

[1] For $\Delta X = 111$ km, the meridional separation at the Equator.

Table 6. Basins defined for objective analysis and the shallowest standard depth level for which each basin is defined.

#	Basin[1]	Standard Depth Level	#	Basin[1]	Standard Depth Level
1	Atlantic Ocean	1*	31	West European Basin	82
2	Pacific Ocean	1*	32	Southeast Indian Basin	82
3	Indian Ocean	1*	33	Coral Sea	82
4	Mediterranean Sea	1*	34	East Indian Basin	82
5	Baltic Sea	1	35	Central Indian Basin	82
6	Black Sea	1	36	Southwest Atlantic Basin	82
7	Red Sea	1	37	Southeast Atlantic Basin	82
8	Persian Gulf	1	38	Southeast Pacific Basin	82
9	Hudson Bay	1	39	Guatemala Basin	82
10	Southern Ocean	1*	40	East Caroline Basin	87
11	Arctic Ocean	1	41	Marianas Basin	87
12	Sea of Japan	1	42	Philippine Sea	87
13	Kara Sea	22	43	Arabian Sea	87
14	Sulu Sea	25	44	Chile Basin	87
15	Baffin Bay	37	45	Somali Basin	87
16	East Mediterranean	41	46	Mascarene Basin	87
17	West Mediterranean	47	47	Crozet Basin	87
18	Sea of Okhotsk	47	48	Guinea Basin	87
19	Banda Sea	55	49	Brazil Basin	92
20	Caribbean Sea	55	50	Argentine Basin	92
21	Andaman Basin	62	51	Tasman Sea	87
22	North Caribbean	67	52	Atlantic Indian Basin	92
23	Gulf of Mexico	67	53	Caspian Sea	1
24	Beaufort Sea	77	54	Sulu Sea II	37
25	South China Sea	77	55	Venezuela Basin	37
26	Barents Sea	77	56	Bay of Bengal	1*
27	Celebes Sea	62	57	Java Sea	16
28	Aleutian Basin	77	58	East Indian Atlantic Basin	97
29	Fiji Basin	82	59	Chiloe	1
30	North American Basin	82	60	Bransfield Strait	37

[1] Basins marked with a "*" can interact with adjacent basins in the objective analysis.

Table 7. Statistical fields calculated as part of WOA23 Salinity
(√ denotes fields were calculated and are publicly available).

Statistical Field	One Degree Fields Calculated	Quarter Degree Fields Calculated	Five Degree Statistics Calculated
Objectively Analyzed Climatology - Annual	√	√	
Objectively Analyzed Climatology - Seasonal	√	√	
Objectively Analyzed Climatology - Monthly	√	√ [1]	
Statistical Mean[2]	√	√	√
Number of Observations	√	√	√
Seasonal (Monthly) Climatology Minus Annual Climatology	√	√	
Standard Deviation from Statistical Mean[2]	√	√	√
Standard Error of The Statistical Mean[2]	√	√	√
Statistical Mean Minus Objectively Analyzed Climatology[2]	√	√	
Number of Mean Values Within Radius of Influence	√	√	
Objectively Analyzed Standard Deviation	√	√	
Standard Error of the Analysis	√	√	

[1] Quarter-degree objectively analyzed monthly climatologies are only available for the climate normal (1971-2000, 1981-2010, and 1991-2020), the 2005-2014 and 2015-2022 decades, and the seven-decade average (1955-2022).
[2] Statistical fields are only available when the objectively analyzed fields are available (for one- and quarter-degree fields).
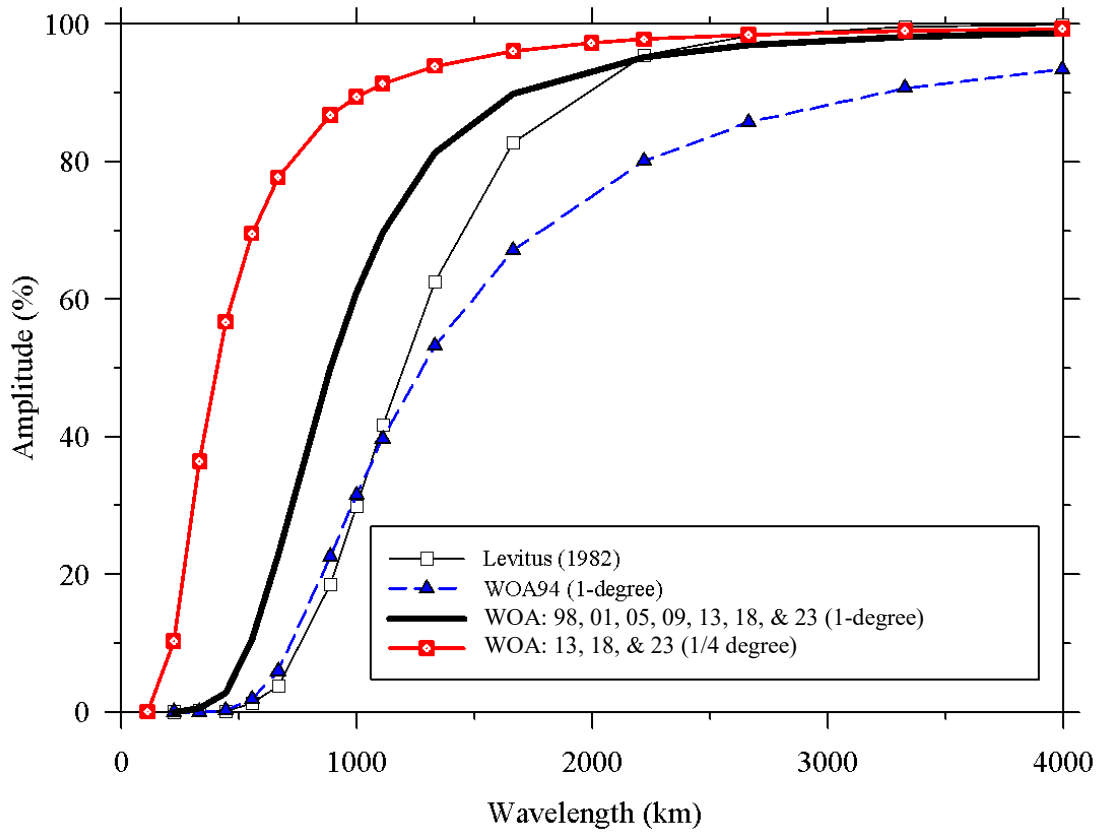
Figure 1. Response function of the WOA23, WOA18, WOA13, WOA09, WOA05, WOA01, WOA98, WOA94, and Levitus (1982) objective analysis schemes.
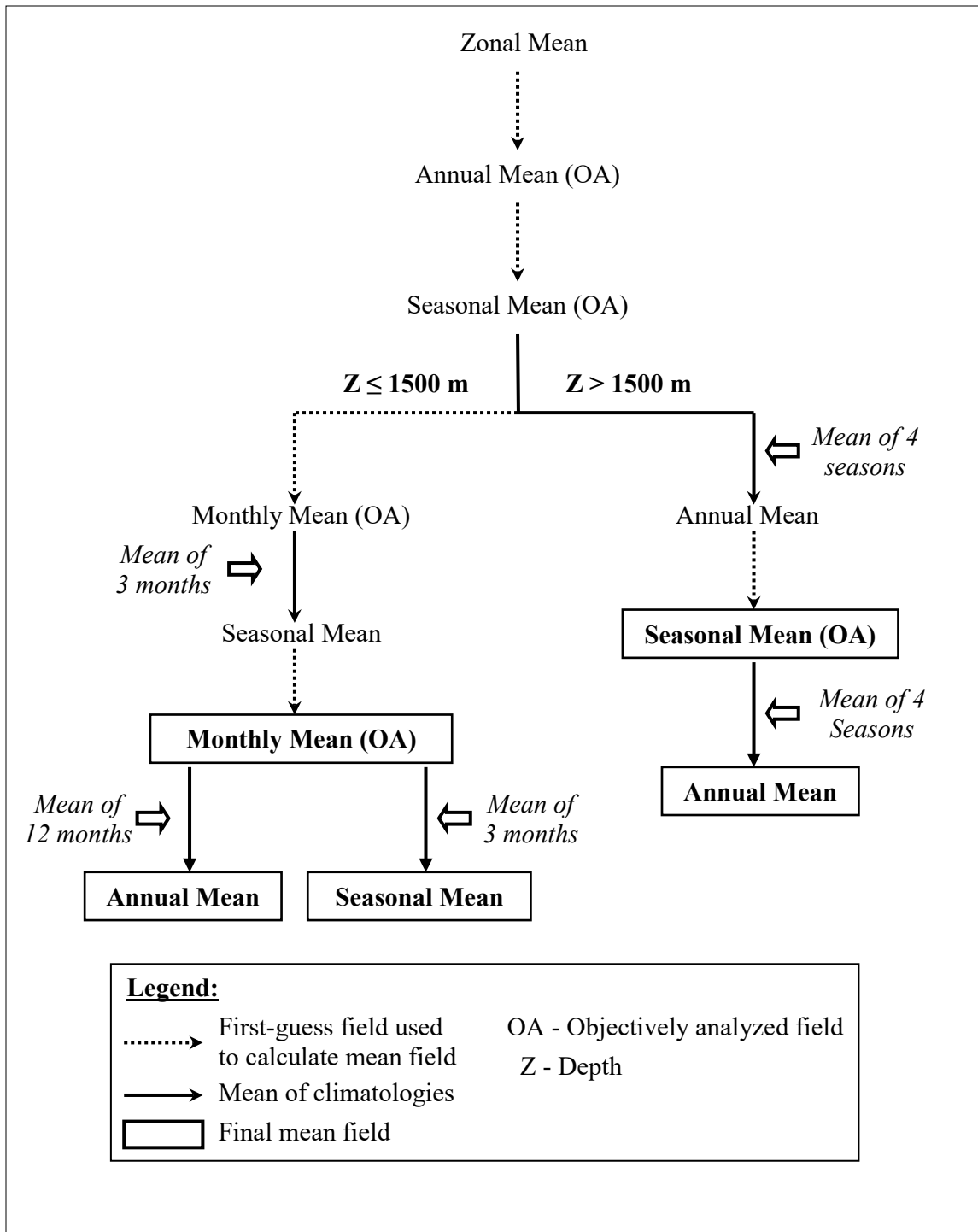
Figure 2. Scheme used in computing "all-data" annual, seasonal, and monthly objectively analyzed means for salinity.

8. APPENDICES

8.1. Appendix A: Stabilization of Temperature and Salinity Climatologies

A1. Defining and identifying instabilities

The first step is to identify the instabilities. The definition of stability is found in section 2.2.4. It will be repeated here for convenience. We use the Hesselberg-Sverdrup criteria described by Lynn and Reid (1968) and Neumann and Pierson (1966). The stability, E, is defined as

$$E = \lim_{\partial z \to 0} \frac{1}{\rho_0} \frac{\delta \rho}{\partial z}$$

in which:
  z = depth,
  ρ = in situ density,
  ρ_0 = 1.02 g·cm^{-3}, and
  $\delta \rho$ = vertical density difference.

As noted by Lynn and Reid, the stability, E, is "the individual density gradient defined by vertical displacement of a water parcel (as opposed to the geometric density gradient). For discrete samples, the density difference ($\delta \rho$) between two adjacent levels is taken after one is adiabatically displaced to the depth of the other."

The computational form for E involves computing the local potential density of the deeper of the two adjacent levels with respect to the depth of the shallower of the two adjacent levels. If this density is lower than the in-situ density at the higher level, this represents an instability. A profile of E is generated from the profiles of objectively analyzed temperature and salinity for each ocean grid box. There will be K-1 values of E in the profile, where K corresponds to the number of depth levels at a given grid point.

If an instability is encountered between two levels, k and k+1, it must be determined whether to change the temperature and/or salinity to achieve stability, and whether to make the change on level k or level k+1. The goal is to change the original climatological profiles of temperature and salinity, and by extension, of density, as little as possible while achieving stability.

A2. Deciding to change temperature and or salinity

Before deciding which level to change, the values of $\Delta T/\Delta z$ and $\Delta S/\Delta z$, the gradients of temperature and salinity between adjacent levels involved in the instability, are examined. This helps determine if the temperature or salinity profile, or both, are to be changed to stabilize the density field. The values of $\Delta T/\Delta z$ and $\Delta S/\Delta z$ are in different units, but some judgments can be made looking at the sign of the values:

If $\Delta T/\Delta z > 0$, $\Delta S/\Delta z > 0$: only temperature is changed.

If $\Delta T/\Delta z < 0$, $\Delta S/\Delta z < 0$: only salinity is changed.
If $\Delta T/\Delta z > 0$, $\Delta S/\Delta z < 0$: local linear trend test employed as described in section A3.

Increasing temperature acts to decrease density (when temperature is above the temperature of the maximum density for the given salinity), decreasing salinity acts to decrease density. If temperature increases while salinity between levels is static or increasing, we assume it is the temperature gradient which is responsible for the instability between these two levels. Conversely, if the salinity is decreasing, while the temperature is static or decreasing, we assume it is the salinity data which are responsible for the noted instability. In the example in Appendix B, instabilities #1, #2.2, #2.3, #5, #6, and #6.1 are stabilized using the results of this gradient test.

In grid boxes where any analyzed temperature in the top 500m of the water column is below freezing, the stabilization will only change salinity values, not temperature. At low temperatures, density depends mainly on salinity and the stabilization routine can produce unrealistic values if temperature is allowed to change. In addition, the stabilization routine will also adjust temperature to the value at the freezing point for the corresponding climatological mean salinity value if the temperature is originally lower than the freezing point. Further details and examples are presented in Boyer et al. (2015).

If temperature is increasing while salinity is decreasing between levels, more information is necessary to understand to what extent temperature and salinity are involved in creating the given instability, as we describe in the next section.

A3. Local linear trend in density

A method we term the "local linear trend in density" is employed. This method is illustrated in instability #2 in the example in appendix B. In this method, the levels k-2 to k+3 from the temperature and salinity profiles at the grid-point containing the instability are used, where k is the upper level involved in the density instability and k+1 is the deeper level. The change in density due to temperature (holding salinity constant) and the change in density due to salinity (holding temperature constant) are estimated for each set of adjacent levels [(k-2,k-1), (k-1,k), (k,k+1), (k+1,k+2), (k+2,k+3)]. The constant values of temperature and salinity used are the average values of these parameters over their entire profiles at the grid-point containing the instability.

The density change due to temperature (salinity) between levels k and k+1 is used as a base value from which the density change due to temperature (salinity) between the other four sets of adjacent levels are subtracted:

$$\text{LLT(T)} = (\Delta \rho_k(T)/\Delta z)_{k,k+1} - (\Delta \rho_{k-2}(T)/\Delta z)_{k-2,k-1} - (\Delta \rho_{k-1}(T)/\Delta z)_{k-1,k} \ (\Delta \rho_{k+1}(T)/\Delta z)_{k+1,k+2} - (\Delta \rho_{k+2}(T)/\Delta z)_{k+2,k+3}$$

$$\text{LLT(S)} = (\Delta \rho_k(S)/\Delta z)_{k,k+1} - (\Delta \rho_{k-2}(S)/\Delta z)_{k-2,k-1} - (\Delta \rho_{k-1}(S)/\Delta z)_{k-1,k} - (\Delta \rho_{k+1}(S)/\Delta z)_{k+1,k+2} - (\Delta \rho_{k+2}(S)/_{\Delta z})_{k+2,k+3}$$

This localized linear trend gives some sense of how the temperature and salinity are changing in the general vicinity of the instability in similar units, and how that change is affecting

the density structure. For instance, if $(\Delta\rho_k(T)/\Delta z)_{k,k+1} < 0$ by only a small amount, and $(\Delta\rho_{k-2}(T)/\Delta z)_{k-2,k-1}$, $(\Delta\rho_{k-1}(T)/\Delta z)_{k-1,k}$, $(\Delta\rho_{k+1}(T)/\Delta z)_{k+1,k+2}$, and $(\Delta\rho_{k+2}(T)/\Delta z)_{k+2,k+3}$ are also < 0, it would appear that the temperature is naturally increasing in the vicinity of the instability and the value of LLT(T) would reflect this by being positive, or only slightly negative. Conversely, if the base $(\Delta\rho_k(S)/\Delta z)_{k,k+1}<0$, while $(\Delta\rho_{k-2}(S)/\Delta z)_{k-2,k-1}$, $(\Delta\rho_{k-1}(S)/\Delta z)_{k-1,k}$, $(\Delta\rho_{k+1}(S)/\Delta z)_{k+1,k+2}$, and $(\Delta\rho_{k+2}(S)/\Delta z)_{k+2,k+3}$ are all > 0, this would indicate the possibility that $(\Delta\rho_k(S)/\Delta z)_{k,k+1}$ may be an anomaly, and the salinity may be the source of the instability. The resultant negative LLT(S) makes this apparent.

Thus,

  If LLT(T) < 0, LLT(S) > 0 : only temperature changed
  If LLT(T) > 0, LLT(S) < 0 : only salinity changed.

  If LLT(T) < 0, LLT(S) < 0 (or LLT(T) > 0, LLT(S) > 0) : the combined linear trend
                                                   test is employed.

The combined linear trend test, which is employed in instabilities #4, #4.1, and #4.2 of the example in appendix B, is as follows:

T_p= LLT(T)/(LLT(T)+LLT(S))*100
S_p= LLT(S)/LLT(T)+LLT(S))*100

Where T_p is percent of change in density due to temperature and S_p is percent of change in density due to salinity

In this case, temperature and salinity are both changed. The change in salinity is responsible for S_p percent of the total change in density needed to achieve stability. The change in temperature is made to account for T_p percent of the total change in density needed to achieve stability.

A4. How temperature and salinity are changed

Once it is determined which variable to change, it is simple to make the change. If the upper level needs to be adjusted, the temperature is increased and/or the salinity is decreased to come as close as possible to $\rho_k(k+1) - \rho_k(k) = 0$. This is the minimum static stability. It is not always possible to reach zero exactly due to the precision limitations of the temperature and salinity values used. The distributed ASCII versions of the temperature and salinity climatologies have four digits to the right of the decimal. So, the maximum significant digits to the right of the decimal for density is also four. As a result, the minimum value for the quantity $\rho_k(k+1) - \rho_k(k) <= |10^{-4}|$. If the lower level needs to be adjusted, the temperature at this level is decreased and/or salinity is increased to reach the minimum static stability. Deciding whether the upper or lower level should be changed is addressed in the next section. Since $\rho_k(k+1)$ is calculated using potential temperature relative to the upper level, it is actually the potential temperature which meets the $\rho_k(k+1) - \rho_k(k) = 0$ requirement, and then from this, the in-situ temperature is determined.

In the case where both the temperature and salinity are changed, temperature is changed first. If the upper level is being adjusted, the temperature which fits the density $\rho_k(k)'$, (where $\rho_k(k)' = \rho_k(k) - ((\rho_k(k+1) - \rho_k(k)) * (T_p/100))$) is calculated. That is, the temperature which changes the density of the upper level T_p percent of the total change in density which is necessary to achieves stability. This temperature is then used to calculate the salinity which achieves minimum static stability.

Similarly, if the lower level is changed, the temperature which fits the density $\rho_k(k+1)' = \rho_k(k+1) + ((\rho_k(k+1) - \rho_k(k)) * (T_p/100))$ is calculated, and then the salinity which, coupled with this temperature approaches $\rho_k(k+1) - \rho_k(k) = 0$, is found.

The temperature is calculated by adding or subtracting small increments to the original temperature until the desired density is approached as closely as possible. The salinity is approximated using the polynomial approximation to the International Equation of State (Levitus and Isayev, 1992) from the given density and temperature, and adding or subtracting small increments until the desired density is approached as closely as possible.

A5. Deciding on changing either upper or lower level

The temperature and/or salinity at only one level need to be changed to achieve static stability (all non-negative values in the E profile). The temperature/salinity change is made at the level which will least affect the overall profiles of temperature and salinity. Both the necessary change at the upper level (k) only and the change at the lower level (k+1) only are calculated. The possible new temperature and/or salinity values at the upper level (k) are used to calculate a new E value between the upper level (k) and the next higher (k-1) level (when possible) to see if a new instability is created. Likewise, a new E value between the lower level and the next lower level (k+2, when possible) is calculated from the proposed new temperature and/or salinity values. If there is a new instability created by changing the upper level, but no new instability created by changing the lower level, the lower level is the level where the temperature and/or salinity changes will be implemented, and vice-versa.

If there are new instabilities in both cases, successively higher levels are checked using the proposed temperature/salinity changes to the upper level involved in the instability, calculating E between the successively higher levels and the upper level with the temperature/salinity changes. The same is done between the lower level with its proposed temperature/salinity values and each successive lower level. This continues one step past either reaching the topmost level or the bottommost level. For instance, if there are nine levels in a profile, and the instability takes place between levels five and six, the proposed temperature/salinity changes to level five and to level six will be checked a maximum of four times for new instabilities. E will be calculated between the lower level and levels seven, eight, and nine, respectively. E will be recalculated between the upper level and levels four, three, two, and one. If there are instabilities all the way to the bottom, this would be equal to instabilities all the way up the water column, to level two. One more check on the upper levels is made, and if this too is an instability, this will be deemed as the upper level proposed temperature/salinity changes creating more instabilities than the lower level proposed temperature/salinity changes, and the temperature and salinities changes to the lower level will be implemented. This test was implemented in all cases in appendix B, except instabilities #2.1 and #5.

If no new instabilities are created, or if the same number of new instabilities are created in both the upper level proposed temperature/salinity changes and the lower level proposed temperature/salinity changes, the smallest necessary change is preferred.

Let $|dt(k)|$ = temperature adjustment to level k (absolute value of original temperature value minus adjusted temperature value.

$|ds(k)|$ = salinity adjustment to level k (absolute value of original salinity value minus adjusted salinity value).

If $|dt(k)| < |dt(k+1)|$ and $|ds(k)| < |ds(k+1)|$: change k   (upper level)
If $|dt(k)| > |dt(k+1)|$ and $|ds(k)| > |ds(k+1)|$: change k+1 (lower level)
If $|dt(k)| > |dt(k+1)|$ and $|ds(k)| < |ds(k+1)|$ or
  $|dt(k)| < |dt(k+1)|$ and $|ds(k)| > |ds(k+1)|$: use adjusted linear trend test

The above test was implemented in examples #2.2 and #5 in appendix B, but only for the trivial case in which only temperature was changed.

The adjusted linear trend (which is not demonstrated in appendix B) is as follows:

The local linear trend in density is computed for temperature and salinity for the case of the change to the upper level (k) and the case of the change to the lower level (k+1). Then the complete adjusted linear, LLTA, is

$LLTA(k) = abs[(LLT(T(k) + dt(k))) + LLT(S(k) + ds(k)))) - (LLT(T(k) + LLT(S(k)))]$

If LLTA(k) < LLTA(k+1) : change k (upper level)
If LLTA(k) >= LLTA(k+1) : change k+1 (lower level)

In other words, the level that is changed is the level which minimizes total change to local linear trends of density with respects to temperature and salinity. In the case where the change is equal, the choice of level to change is ambiguous and the level changed is arbitrarily set to the lower level.

A6. Finalizing temperature and salinity profiles

Each E profile is checked for instabilities starting at the surface and then proceeding to the bottom, or the 102nd standard level (5500 meters), whichever is reached first. If an instability is encountered, it is dealt with as detailed above. If this process results in a new instability involving the upper layer involved in the old instability and the level above that one, this new instability is dealt with before proceeding further down the profile. This process is continued until there are no instabilities in the entire E profile. It may be that the temperature and salinity at a level are changed numerous times in the process of stabilizing the entire E profile. This may be necessary to achieve the minimum possible changes over the entire temperature and salinity profiles while still creating stability.

Then the procedure is performed again on the original E profile, this time starting from the

bottom of the profile and continuing to the surface. There are grid boxes which have large gradients in temperature and/or salinity near the surface. If these large gradients are involved in an instability, and the E profile is being checked from the top down, these large gradients may propagate changes down to lower depths when they should be confined to the upper depths. When the profile is checked from the bottom up, the lower depths are usually preserved intact while changes are made only in the upper layer.

Finally, the density change due to temperature and to salinity is calculated for the top-down and the bottom-up cases. The density change from the original profile due to temperature is calculated at each level, as is the density change from the original profile due to salinity.

The density changes at each level are added together and divided by the number of levels minus one to get an average density change for both the top-down case and the bottom-up case. The case with the lowest average density change is the case implemented. If average density change is equal in both cases, the top down case is implemented.

8.2. Appendix B: Example of Stabilization

The area chosen for this example is the one-degree latitude-longitude box centered at 53.5°S -171.5°E from a previous version of the World Ocean Atlas (1998, WOA98). This is on the New Zealand Plateau, with a bottom depth below 1000 meters and above 1100 meters. The month is October, during the early austral summer. There is a deep mixed layer in this area, using vertical temperature change as an indicator. There is no temperature or salinity data within the chosen one-degree box. Thus, the objectively analyzed values in this one-degree box will be dependent on the seasonal objectively analyzed field and the data in near-by one-degree grid boxes. There is much more temperature data than salinity data on the New Zealand plateau for October. This contributes to six small (on the order of 10^{-2} kg·m^{-3}) inversions in the local potential density field calculated from objectively analyzed temperature and salinity fields. The whole numbers in bold below correspond to the numbered instability shown in Table B1 and Table B2. The decimal numbers in bold shown in Table B2 correspond to new instabilities created while correcting the original instabilities. Table B2 shows the final, stabilized profiles.

#1. Working first from the bottom of the profile upwards, the first inversion is encountered between 400 and 500 m depth. The temperature rises with the increase in depth here, from 6.8275°C to 7.4001°C, while the salinity increases from 34.2852 PSS to 34.3123 PSS. Using the criteria of the gradient test, the temperature will be changed here, while the salinity will not. Now it remains to decide whether to change the temperature value at 400 m or 500 m. If the temperature value at 400 m is changed to eliminate the instability, a new instability will be created between 300 m and 400 m depth. No new instability is created if the value at 500 m depth is changed. Therefore, the temperature value at 500 m depth is changed to 6.9838°C to create a situation where the stability is within 10^{-4} kg·m^{-3} of neutral stability.

#2. Continuing upwards, the next instability is found between 250 and 300 m depth. The temperature here rises from 7.0962°C to 7.1622°C. The salinity decreases from 34.3415 PSS to 34.3367 PSS. The gradient test cannot be used in this case, since both temperature and salinity are acting to decrease stability. The next test, the local linear trend in density must be implemented.

This test ascertains the general tendency of the temperature and salinity in the immediate area of the instability. Is the temperature generally increasing? Is the salinity generally increasing? In this case, the levels to be checked, listed by depths are:

k-2 = 150 m depth,   t(k-2) = 6.8919°C,   s(k-2) = 34.3697 PSS (instability)
k-1 = 200 m depth,   t(k-1) = 6.9363°C,   s(k-1) = 34.3364 PSS (instability)
k   = 250 m depth,   t(k)   = 7.0962°C,   s(k) = 34.3415 PSS(instability)
k+1 = 300 m depth,   t(k+1) = 7.1622°C,   s(k+1)= 34.3367 PSS
k+2 = 400 m depth,   t(k+2) = 6.8275°C,   s(k+2)= 34.2852 PSS
k+3 = 500 m depth,   t(k+3) = 6.9838°C,   s(k+3)= 34.3123 PSS

It is already known that the changes in both temperature and salinity between k and k+1 work to decrease stability, otherwise, this test would not be needed. Therefore, the density change between levels k and k+1 keeping salinity constant is negative. The test is to see how large is the density change between levels k and k+1 in relation to the cumulative density changes between other adjacent levels, keeping salinity constant. The density changes between levels k-2 and k-1, and between levels k-1 and k are not used in this test for this case because the density structure between these adjacent levels are unstable and therefore assumed to include anomalous temperature and/or salinity values. The density change due only to temperature between levels k+1 and k+2 is positive and fairly large in comparison with the instability between k and k+1. The density change between levels k+2 and k+3 is negative. However, the cumulative valid density changes due only to temperature between adjacent levels in the immediate area of the instability between levels k and k+1 is positive and slightly larger in comparison with the absolute value of the instability between levels k and k+1. To get a numerical value for this comparison, the cumulative value of valid density changes due to temperature between adjacent levels in the immediate area of the instability between levels k and k+1 is subtracted from the value of the density change between levels k and k+1. If the result is positive, this denotes that the gradient of the temperature in the immediate area of the instability is of the same sign as the temperature gradient between levels k and k+1. This reinforces the idea that the temperature gradient between levels k and k+1 is probably not an anomaly, but follows the true pattern of the temperature profile. If the result is negative, this denotes that the temperature gradient between levels k and k+1 does not follow the pattern of adjacent areas of the temperature profile and is probably an anomaly.

Looking at the change in density between adjacent levels due to salinity, the change between levels k+1 and k+2 is quite large in comparison to the density change due to salinity between the levels k and k+1, where the instability occurs. The change between levels k+2 and k+3 in density due to salinity is negative and smaller in absolute value than the increase between levels k+1 and k+2.

The results for the local linear trend test in density for temperature and salinity are negative and positive respectively. These results lead to a change in temperature in either level k or level k+1 to rectify the instability. This is not the optimal trial for the local linear trend in density test because two of the four adjacent level density changes could not be used due to their own instabilities. If either the upper (k) value for temperature or lower (k+1) value is changed, new instabilities will result in the profile. In the case where instabilities already exist, (the upper level temperature value

37

changed) the instabilities are exacerbated. But more levels will be affected if the upper level temperature value is changed. So, the lower level (k+1) temperature value is changed to eliminate the instability between levels k and k+1. The new value at 300 m depth for temperature is 7.0748°C.

#2.1, #2.2. Because of this change, there is now an instability between 300 and 400 m depth. The gradient test reveals negative gradients in temperature and salinity. This leads to a new salinity value of 34.2894 PSS (from an old value of 34.2852 PSS) at 400 m depth. Temperature is unchanged. This causes a new instability between 400 and 500 m depth. The gradient test indicates a change only to temperature. Since neither a change to the upper level or lower level will cause new instabilities, a temperature change to the lower level is implemented because it incurs a smaller change to the temperature at that level than would the change to the upper level. The new temperature value at 500 m depth is 6.9604°C (old value 6.9838°C).

#3. Since no new instabilities were created in the last change, checking proceeds up the profiles again. The next instability occurs between 200 and 250 m depth. The result of the gradient test and choosing the minimum change to the original values, is to change the temperature only, at 200 m depth, from 6.9363°C to 7.0628°C.

#4. The instability between 150 and 200 m depth cannot be resolved using the gradient test. The following levels are set for the local linear trend in density test:

$$
\begin{array}{lll}
k\text{-}2 = 100 \text{ m depth,} & t(k\text{-}2) = 6.9753°C, & s(k\text{-}2) = 34.3280 \text{ PSS} \\
k\text{-}1 = 125 \text{ m depth,} & t(k\text{-}1) = 6.9218°C, & s(k\text{-}1) = 34.3604 \text{ PSS} \\
k \ \ = 150 \text{ m depth,} & t(k) \ \ = 6.8919°C, & s(k) \ = 34.3697 \text{ PSS (instability)} \\
k\text{+}1 = 200 \text{ m depth,} & t(k\text{+}1) = 7.0628°C, & s(k\text{+}1)= 34.3364 \text{ PSS} \\
k\text{+}2 = 250 \text{ m depth,} & t(k\text{+}2) = 7.0962°C, & s(k\text{+}2)= 34.3415 \text{ PSS} \\
k\text{+}3 = 300 \text{ m depth,} & t(k\text{+}3) = 7.0748°C, & s(k\text{+}3)= 34.3367 \text{ PSS.}
\end{array}
$$

Since this is an iterative process, the values for temperature at 250 and 300 m depth are the newly calculated values, not the original values.

In this case, the density with respects to temperature increases between levels k-2 and k-1, between k-1 and k, and between k+2 and k+3. This is not completely offset by the decrease in density due to temperature between levels k+1 and k+2. So the numerical value for temperature for the local linear trend in density is negative. For density with respects salinity, the value is positive for all adjacent levels except between k+2 and k+3. The local linear trend in density for salinity is also negative. So, this test is also inconclusive.

When this point is reached, both temperature and salinity will be changed. The extent to which they will be changed depends on their relative local linear trends in density. This is the reason for computing the local trends of temperature and salinity in like units. The local linear trend in density for temperature is -0.0357 kg·m^{-3}. The local linear trend in density for salinity is - 0.0592 kg·m^{-3}. Using their ratio, 62% of the change in density necessary for stabilization will be accounted for by changing the salinity, 38% will be accounted for by changing the temperature. Changes on the upper level are found to cause fewer new instabilities than changes to the bottom level. The new values for 150 m depth are 7.0242°C for temperature and 34.3301 PSS for salinity.

#4.1. A new instability is created between 125 and 150 m depth. Again, both the gradient test and the local linear trend in density are inconclusive. Both temperature and salinity are changed, with salinity accounting for 75% of the change in density. The values at 125 m depth are changed from 6.9218°C to 6.9897°C for temperature and 34.3604 PSS to 34.3243 PSS for salinity.

#4.2. A new instability between 100 and 125 m depth is again resolved only by changing both temperature and salinity at 100 m. The new values are 6.9796°C and 34.3228 PSS for the respective variables (old values 6.9753°C and 34.3280 PSS).

#5, **#6, #6.1.** The final two original instabilities, between 50 and 75 m depth and between 10 and 20 m depth are both resolved by the gradient test. The level of the change for the former instability is chosen on the basis of least change to the temperature, since no new instabilities are created. In this case the value of temperature at 50 m depth is changed from 6.9686°C to 7.0132°C. For the latter case, the value of salinity at 10 m depth is changed from 34.4278 PSS to 34.3063 PSS. This creates one last instability between the surface and 10 m depth. The gradient test yields a change in the surface salinity from 34.4243 PSS to 34.3096 PSS. The level at which the change is made is based on the change which creates the fewest new instabilities.

A complete, altered, stable set of temperature and salinity profiles has now been achieved.

The entire process is repeated starting from the top and proceeding downwards through the profile. The changes to density at each level are calculated for the results of the top-down and bottom-up calculations. The procedure which cumulatively changes the original density structure least is chosen as the final result. The reason for doing both top-down and bottom-up procedures is that when there is a large instability near the surface, doing the top-down procedure can significantly alter the entire profile set, whereas bottom-up will confine the changes to the near surface portion. The converse is also true. So, both procedures are performed to identify the procedure which changes the original the least.

The chosen profile is an extreme example of the stabilization process, used to illustrate all aspects of the procedure. Each instability is initially treated separately, and a single level in a profile may be altered many times due to changes in the surrounding levels before a fully stable set of temperature and salinity profiles is produced.

Table 8. Grid box 171.5°E, 53.5°S Improved WOA98 profiles before stabilization

Depth (m)	Temp (°C)	Salinity	ρ (kg·m⁻³)	ρ (kg·m⁻³)	E (kg·m⁻³)	Change #
0.0	7.1667	34.4243	26.9423	26.9476	0.0054	
10.0	7.1489	34.4278	26.9939	26.8982	-0.0957	**#6**
20.0	7.0465	34.2880	26.9443	26.9529	0.0085	
30.0	7.0050	34.2914	26.9990	27.0104	0.0114	
50.0	6.9686	34.2991	27.1028	27.0967	-0.0061	**#5**
75.0	7.0604	34.3073	27.2120	27.2406	0.0286	
100.0	6.9753	34.3280	27.3560	27.3892	0.0332	
125.0	6.9218	34.3604	27.5046	27.5164	0.0117	
150.0	6.8919	34.3697	27.6316	27.6000	-0.0316	**#4**
200.0	6.9363	34.3364	27.8302	27.8123	-0.0179	**#3**
250.0	7.0962	34.3415	28.0421	28.0295	-0.0126	**#2**
300.0	7.1622	34.3367	28.2593	28.2684	0.0092	
400.0	6.8275	34.2852	28.7281	28.6664	-0.0618	**#1**
500.0	7.4001	34.3123	29.1238	29.3699	0.2461	
600.0	6.2133	34.4022	29.8292	29.9386	0.1094	
700.0	5.9186	34.4868	30.3978	30.5869	0.1891	
800.0	4.5426	34.4904	31.0488	31.0754	0.0266	
900.0	4.1263	34.4558	31.5377	31.6539	0.1162	
1000.0	3.3112	34.4755	32.1176			

Table 9. Grid box 171.5°E, 53.5°S Improved WOA98 profiles after stabilization

Depth (m)	Temp (°C)	Salinity	ρ (kg·m⁻³)	ρ (kg·m⁻³)	E (kg·m⁻³)	Change #
0.0	7.1667	34.3096	26.8519	26.8521	0.0002	**#6.1**
10.0	7.1489	34.3063	26.8982	26.8982	0.0000	**#6**
20.0	7.0465	34.2880	26.9443	26.9529	0.0085	
30.0	7.0050	34.2914	26.9990	27.0042	0.0051	
50.0	7.0132	34.2991	27.0967	27.0967	0.0000	**#5**
75.0	7.0604	34.3073	27.2120	27.2361	0.0240	
100.0	6.9796	34.3228	27.3513	27.3513	0.0000	**#4.2**
125.0	6.9897	34.3243	27.4667	27.4667	0.0000	**#4.1**
150.0	7.0242	34.3301	27.5820	27.5820	0.0000	**#4**
200.0	7.0628	34.3364	27.8123	27.8123	0.0000	**#3**
250.0	7.0962	34.3415	28.0421	28.0422	0.0000	**#2**
300.0	7.0748	34.3367	28.2719	28.2719	0.0001	**#2.1**
400.0	6.8275	34.2894	28.7314	28.7314	0.0000	**#1, #2.2**
500.0	6.9604	34.3123	29.1899	29.3699	0.1799	
600.0	6.2133	34.4022	29.8292	29.9386	0.1094	
700.0	5.9186	34.4868	30.3978	30.5869	0.1891	
800.0	4.5426	34.4904	31.0488	31.0754	0.0266	
900.0	4.1263	34.4558	31.5377	31.6539	0.1162	
1000.0	3.3112	34.4755	32.1176			

8.3. Appendix C: Geographic salinity limitations

As was discussed in section 3.2, the objective analysis of in situ salinity data to build the World Ocean Atlas 2023 is strongly dependent on the first-guess field and the density of observations surrounding the grid point of interest. For most of the global ocean, there are sufficient salinity data for each season when all data over the entire time period of record in WOD23 are used (Mishonov *et al.,* 2024). This allows us to compute accurate and seasonal-specific "all-data" first guess fields.

However, in two climatically-important portions of the World Ocean, the Arctic and Southern Oceans, data distributions are extremely infrequent, spatially sparse, and strongly seasonally-biased. For example, the Arctic Ocean is much better sampled in boreal summer when retreat of sea ice allows ships to navigate further into the interior and deploy various onboard instruments to measure in situ seawater salinity. Additionally, during the warmer months, melting sea ice and river runoff is at their peaks thus strongly freshening much of the near-surface open-ice water. Therefore, this seasonally-biased data distribution in the Arctic Ocean results in a very fresh near-surface "all-data" first-guess field. Moreover, due to brine rejection from freezing sea ice and no ongoing melting, any winter salinity observations that do exist yield typically much higher values than what is in the first-guess salinity field. Using such biased first-guess fields in the objective analysis procedure results in artificially high salinities during winter in some portions of the Arctic Ocean. With such artificially elevated near-surface salinity and fresher subsurface salinity, combined with near uniform temperature (yielding a very unstable profile), the stabilization procedure can incorrectly alter winter salinity in those portions of the Arctic Ocean. While the stabilization procedure normally does help to lower the near-surface salinities in some of these artificially salty areas, it also can create some discontinuities in the stabilized temperature and salinity fields. We recognize this issue and are actively working to address it as soon as we can. Yet it remains a difficult task in view of still severe sparseness of data, particularly in winter. As the volume of the Arctic Ocean data in WOD continues to increase, there is a hope that the salinity climatologies in this region can be improved and the issue with seasonal biases will be properly addressed.

The above example is just one of a few regions that may be seriously impacted by data sparsity, temporal or spatial, and/or by seasonal bias issues. Because of its remoteness, vastness, and severe weather conditions, especially in boreal winter, the Southern Ocean data are also prone to the same issue, as are some marginal seas (e.g., South China Sea). Therefore, depending on the region being investigated, careful inspection of the data distribution, statistical fields, and objectively analyzed fields (all available in this atlas) is advised, especially in regions where this issue may be a priori suspected.

8.4. Appendix D: Adjusting regions of large stabilization change

As discussed in section 3.5.1, there are a few regions that underwent large changes in subsurface salinity as a direct result of stabilization. One such example is in February of the 1955-1964 decade. There were a few anomalously cold temperature observations (likely due to an equatorward shift of the Subantarctic Front) in the South Central Indian Ocean in February during the 1955-1964 decade. These observations were only present in the upper 250m, which made the

upper layers quite cold. Since this was the only data in this area, the cold temperatures stretched both north, south, east, and west after the objective analysis. Thus, with cold temperatures in the upper 250m, and warmer temperatures below it made for a large inversion. This large inversion was stabilized during the stabilization process, and in order for the water below 250m (which was warmer than the water above) to be stabilized with the water above, salinity was increased from 250m through 800m.

To fix this issue we had to incorporate additional observations into the objective analysis. Thus, we took the decadal seasonal statistical mean field for which the monthly statistical mean was a part of (e.g., Boreal 1955-1964 Winter was chosen for 1955-1964 February), and added those seasonal statistical means into the monthly field. The objective analysis and stabilization were then rerun and the resulting fields looked much cleaner. The following areas were impacted through this process:

1. 1955-1964 February: Statistical means from Winter 1955-1964 were added to the February statistical mean for latitude-longitude boxes:
   a. 72E-82°E, 39S-46°S
   b. 21E-30°E, 35S-42°S
2. 1965-1974 December: Statistical means from Fall 1965-1974 were added to the December statistical mean for latitude-longitude box:
   a. 112-120°E, 37-49°S
3. 1975-1984 May: Statistical means from Spring 1975-1984 were added to the May statistical mean for latitude-longitude box:
   a. 51-61°E, 41-47°S
4. 1975-1984 September: Statistical means from Summer 1975-1984 were added to the September statistical mean for latitude-longitude box:
   a. 35-63°E, 34-53°S
5. 1985-1994 September: Statistical means from Summer 1985-1994 were added to the September statistical mean for latitude-longitude box:
   a. 21-32°E, 31-42°S
6. 1985-1994 December: Statistical means from Fall 1985-1994 were added to the December statistical mean for latitude-longitude box:
   a. 3-8°E, 30-36°S